Clusterin-targeted bioengineered nanoparticles for sensitizing breast cancer cells to conventional chemotherapy

Andreia Susete Ferreira de Faria
Master in Applications in Biotechnology and Synthetic Biology
Department of Biology and Department of Chemistry and Biochemistry
Faculty of Sciences of the University of Porto
2024

Clusterin-targeted bioengineered nanoparticles for sensitizing breast cancer cells to conventional chemotherapy

Andreia Susete Ferreira de Faria

Dissertation carried out as part of the Master in Applications in Biotechnology and Synthetic Biology
Department of Biology and Department of Chemistry and Biochemistry
2024

Supervisor
Tiago dos Santos, Junior Researcher, i3S

Co-supervisor
Pedro Granja, Group Leader, i3S

Co-supervisor
Marilina García-Aranda, Visiting Researcher, Hospital Universitario Costa del Sol

INSTITUTO
DE INVESTIGAÇÃO
E INOVAÇÃO
EM SAÚDE
UNIVERSIDADE
DO PORTO

Para os meus pais, sempre.

Acknowledgements

First and foremost, I thank God for guiding me to this incredible opportunity to work on a project that means so much to me, in ways words cannot fully express. This journey has been more than academic; it has allowed me to grow both as a researcher and as a person, alongside the remarkable people of the Biofabrication Research Group.

My deepest gratitude goes to Dr Pedro Granja, my co-supervisor and group leader, for welcoming me into his team and for his unwavering support. His open-mindedness, kindness, and invaluable guidance have been fundamental to my development. I am also immensely grateful to my supervisor, Tiago dos Santos, whose patience, knowledge, and encouragement taught me everything I know about cell culture and nanoparticles. His calm and positive attitude, even in the face of challenges, were crucial, always reminding me to embrace the process of "Science being Science."

I am also deeply thankful to my co-supervisor, Marilina García-Aranda, whose enthusiasm and expertise inspired this project. Her energy and insightful advice helped shape this work every step of the way. To my colleague Silvia Sai, thank you for being a thoughtful and dedicated collaborator, always eager to innovate and learn. Your kindness and thoroughness in everything we did together made this project a pleasure.

I am grateful to Caio, Filipa, and Sara for warmly welcoming me into the team and for their genuine support. My sincere thanks also go to Tiago and Marlene Soutelo, my colleagues at McDonald's, who were tirelessly flexible with my schedule to allow me to balance work and research.

To my dear friend Carlos Pinto, a constant source of support throughout this journey, and to my friends Daniel and Laura, who encouraged me to return to academia, I owe you my deepest thanks. I am also grateful to all my friends who prayed for me and uplifted me along the way.

Finally, to my family—especially my sister Maria José, my niece Débora, and my brother-in-law António—thank you for being my cornerstone, offering me the time, space, and support I needed to pursue this path. None of this would have been possible without your love and encouragement.

Abstract

This thesis investigates the potential of PLGA nanoparticles (NPs) loaded with antisense oligonucleotides (ASO) targeting the clusterin (CLU) gene to enhance sensitivity of breast cancer cells to chemotherapeutic agents. Through physicochemical characterization, the encapsulation of ASO demonstrated notable influences on NP size, zeta potential, and aggregation tendencies, particularly with increasing ASO concentrations. These modifications highlighted the role of nucleotide mismatches in modulating NP behaviour, shedding light on the structural effects of ASO on nanoparticle stability.

In vitro assays on MCF7, MDA-MB-231, and SKBR3 breast cancer cell lines revealed that CLU-targeted ASO NPs did not significantly enhance cytotoxic sensitivity to chemotherapy across cell lines, though slight improvements were noted in HER2-positive cells. While promising in its approach, this study underscores the need for optimization in NP synthesis and ASO encapsulation to maximize therapeutic benefits. These findings advance the understanding of CLU-targeted therapy in breast cancer but call for refined strategies to harness the full potential of ASO-loaded PLGA nanoparticles.

Keywords: PLGA nanoparticles (NPs), antisense oligonucleotides (ASO), clusterin (CLU), breast cancer, chemoresistance, MCF7, MDA-MB-231, SKBR3, zeta potential, targeted therapy, nanomedicine, drug delivery systems, chemotherapy sensitization

Table of Contents

List of Tables

List of Figures

List of abbreviations

A	**Adenine**
ASO	**Antisense Oligonucleotide**
C	**Cytosine**
CLU	**Clusterin**
DLS	**Dynamic Light Scattering**
DMEM	**Dulbecco's Modified Eagle Medium**
DNA	**Deoxyribonucleic Acid**
DOX	**Doxorubicin**
ds DNA	**Double-Stranded Deoxyribonucleic Acid**
DTX	**Docetaxel**
EDL	**Electric Double Layer**
EPR	**Enhanced Permeability and Retention**
ER	**Oestrogen Receptor**
FBS	**Foetal Bovine Serum**
FDA	**Food and Drug Administration**
G	**Guanine**
HER2	**Human Epidermal Growth Factor Receptor 2**
IC50	**Inhibitory Concentration 50**
mRNA	**Messenger Ribonucleic Acid**
nCLU	**Nuclear Isoform of Clusterin**
NNI	**National Nanotechnology Initiative**
NPs	**Nanoparticles**
nTPM	**Normalized Transcripts Per Million**
PBS	**Phosphate-Buffered Saline**
PLGA	**Poly-Lactic-co-Glycolic Acid**
PR	**Progesterone Receptor**
PTX	**Paclitaxel**
RNA	**Ribonucleic Acid**
sCLU	**Secretory Isoform of Clusterin**
ss DNA	**Single-Stranded Deoxyribonucleic Acid**
T	**Thymine**
TEM	**Transmission Electron Microscopy**

TNBC	**Triple-Negative Breast Cancer**
TNF	**Tumour Necrosis Factor**
VEGF	**Vascular Endothelial Growth Factor**

1. State of the Art

1.1. Nanoscience, Nanotechnology, Nanoparticles and Nanomedicine

Originating from the Greek, the prefix “nano” that means “dwarf”, is used to represent the measurement of one billionth of a meter (10^{-9} m). For instance, a single human hair has a thickness of approximately 60000 nanometres (nm), while the radius of the Deoxyribonucleic Acid (DNA) double helix, measures about 1 nm, as it is depicted in Fig. 1 [1].

It is crucial to differentiate between nanoscience and nanotechnology: “nanoscience is the study of structures and molecules on the scales of nanometres, ranging between 1 and 100, and the technology that utilizes it in practical applications such as devices etc. is called nanotechnology” [1]. Nanoscience converges physics, biology and materials sciences approaching the manipulation of materials at a molecular and atomic level.

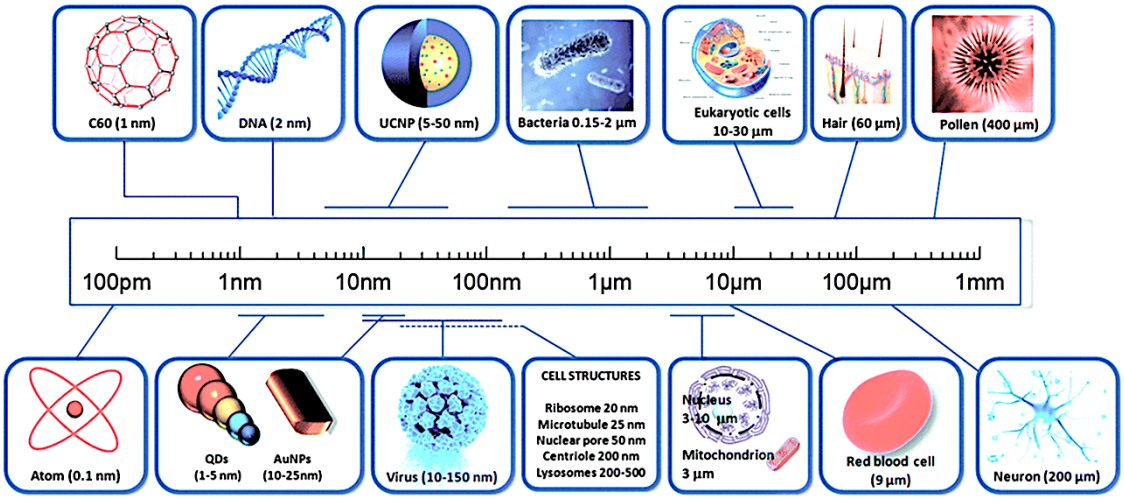

Figure 1 - A comparison of sizes of different structures (adapted from reference [1]).

Being one of the most promising technologies of the 21st century, nanotechnology is defined, by the National Nanotechnology Initiative in the USA, as “the understanding and control of matter at the nanoscale, at dimensions between approximately 1 and 100 nanometres, where unique phenomena enable novel applications” [2], in a broad range of fields, such as chemistry, physics, biology, medicine, engineering and electronics [1]. Nanostructured materials present properties that differ significantly from those same

materials structured at a larger scale, properties such as melting-point, electric conductivity, fluorescence, chemical reactivity and magnetic permeability [3, 4]. This finding is of pivotal importance to nanoscience and nanotechnology since it is at the basis of the fact that one can fine-tune certain material's properties by changing the size of the particle. One great advantage of the nanoparticles is their extremely high surface areas, due to their reduced size. For instance, a solid cube with 1 cm on a side has a surface area of 6 cm^2, like half a stick of gum, but when divided into much smaller cubes with 1 nm on a side, the same volume's surface expands to 6,000 m^2, which is an area larger than a football field. This increased surface area enhances reactivity, making nanoparticles ideal for improving catalysts, such as in car catalytic converters, which now require less precious metal. This principle is also applied in designing advanced batteries, fuel cells, and cleaner energy systems, where increased surface interaction enhances efficiency [2, 3]. Going deeper in the context of this thesis, at biological level, many of the cellular processes naturally occur at the nanoscale level, *e.g.* the haemoglobin, protein that carries oxygen inside erythrocytes through the body, has a diameter of 5.5 nm and, as represented in figure 1, the diameter of one strand of DNA molecule, one of the building blocks of life, measures 2 nm. This understanding of natural occurrence of processes at nano scale level [5], is leading to major developments in fields such as computing systems or energy: for instance, investigation on the use of self-assembly molecules, self-organization and quantum mechanics has permitted the creation of new computing platforms, and in search for clean energy sources, artificial systems for photosynthesis have been created, inspired by nature, and are able to capture and harness energy from the sun [2, 6-8]. The medical field has also benefited from knowledge around nanoscience, nanomaterials and nanotechnology: many researchers are devoting their attention and efforts to develop tools, at the nanoscale level, to be used in treatments, diagnosis and/or therapies, with the advantages of being more precise and personalized than the conventional methods [2, 6, 9, 10].

1.1.1. Nanoscience and Nanotechnology: a gateway to Nanomedicine

The growing interest in applying knowledge of nanoscience and nanotechnology to the medical field, led to the rise of nanomedicine [2, 6, 8, 11, 12], having the approval, by Food and Drug Administration (FDA) in USA, of the first nanotherapeutic drug – Doxil®, an anticancer drug which uses PEGylated liposomes – set the dawn of this new field, back in 1995 [12, 13].

1.1.1.1. Definition and Applications of Nanomedicine

"Most broadly, nanomedicine is the process of diagnosing, treating, and preventing disease and traumatic injury, relieving pain, and preserving and improving human health, using molecular tools and molecular knowledge of the human body. In short, nanomedicine is the application of nanotechnology to medicine [14]." This is the definition found in the review article: "What is Nanomedicine?" from Robert A. Freitas Jr., published in 2005, and is still very complete, although since then, one could observe that nanomedicine has evolved and grown steadily [11, 12, 15]. Aiming to improve existing treatments, nanomedicine has resorted to the employment of nanocarriers, often reformulated from conventional drugs, to reduce side effects and increase drug stability [12]. Recent nanomedicine applications have shown notorious progress in drug delivery, diagnostic precision, and even regenerative medicine, highlighting that this field can give us new treatment pathways by enhancing the nanoscale unique physicochemical properties, that enlarge bioavailability and provide precise molecular mediations [8]. Despite regulatory and translational challenges, nanotechnology's integration into healthcare is moving towards new therapeutical paradigms [12]. Especially fields like oncology, have seen substantial advances due to nanomedicine developments [12, 16]. For instance, targeted delivery systems allow nanoparticles to selectively target cancer cells, reducing conventional side effects and increasing treatment efficacy. These developments lead to a shift from traditional therapies, which usually lack the specificity that complex diseases like cancer need [17]. This refinement of drug delivery and disease diagnose is opening a path toward progressively personalized, effective and secure medical procedures, aiming to reach the point of tailoring treatments to individual patient profiles [8, 11, 15]. Particularly within oncology, nanomedicine became a cornerstone of this personalized therapy, owing to the development of stimuli-responsive and multifunctional nanoparticles, which includes advanced NPs modifications that can adapt to varying physiological conditions, and support the therapeutic precision that is crucial to address both the inherent complexity of cancer diseases and the specific patient needs [11].

1.1.1.2. Types of NPs Used in Anticancer Therapies

NPs have become an elemental tool in cancer therapy due to their unique physicochemical properties, which improve drug delivery, reducing off-target toxicity, and enhancing therapeutic efficiency. Usually categorized based on respective composition, NPs may include polymeric, liposomal, and metal-based types, presenting each one of

these types, distinctive advantages that can be suited to specific therapeutic applications [18, 19]. Here are resumed some characteristics of these main types of NPs:

1. Polymeric NPs

This kind of NPs, particularly the ones made from poly (lactic-co-glycolic acid) (PLGA), are well-known for their biodegradability and biocompatibility. Besides having FDA approval, PLGA's safe degradation into lactic and glycolic acid promote this polymer as ideal for biomedical use, enabling controlled and sustained drug release [19-21].

The delivery of drugs, particularly chemotherapeutic agents, and of biomolecules, *e.g.* nucleic acids for gene therapies, using PLGA NPs, has broadly increased, especially because of their compliant surface properties, which allow modifications, that enable them for targeted delivery, making their use advantageous by reducing adverse side effects. For instance, the delivery of docetaxel (DTX) and paclitaxel (PTX), has been carried out utilizing PLGA NPs as vectors, thus enhancing drug stability and respective efficacy against solid tumours [19, 22].

Additionally, it has been observed an increasing use of PLGA NPs formulations in clinical trials, particularly aiming to target specific cancers, namely triple-negative breast cancer (TNBC) and glioblastoma [18, 21].

2. Liposomal NPs

Liposomal NPs are lipid-based vesicles that can encapsulate both hydrophilic and hydrophobic molecules. They show some characteristics that make their use advantageous and suited for systemic cancer therapies, namely their biocompatibility and capacity to escape from the immune system, which highly increases their bioavailability. Due to the enhanced permeability and retention (EPR) effect, liposomes are permitted to accumulate preferably in tumour tissues, thus reducing systemic exposure and improving treatment efficacy [20, 22].

Some liposomal formulations have been approved for use as cancer treatments. For instance Doxil®, which was the first nano-drug approved by FDA [13], is a liposomal form of doxorubicin (DOX) and is approved for the treatment of cancers such as breast and ovarian cancers. One of the side effects of treatment with free DOX is cardiotoxicity, which is reduced when administrated as Doxil® (DOX encapsulated in a liposome), making the profile of this treatment safer, which represents a notable advancement in chemotherapeutic treatments [19, 21].

3. Metal-Based NPs

Some inherent characteristics of metal-based NPs, such as photothermal properties of gold and magnetic properties of iron oxide, have made their use notorious [19, 20], both in therapeutic and diagnostic functions, giving them great potential in the development of fields such as theragnostic [19], which is an emergent field that combines these two functions, enabling non-invasive imaging methods accompanying specific delivery of therapies [23, 24]. As for photothermal therapies, that uses heating activated by laser to induce localized tumour cell death, has recurred to the utilization of gold NPs, iron oxide NPs have been used as contrast agents in imaging, assisting in both diagnostic and therapeutic applications [19, 20].

4. Additional Emerging Nanoparticles

Besides these mentioned main types of NPs, other relevant types have been developed, worthy of reference at this context, such as:

- Dendrimers, which are globular and hyperbranched synthetic macromolecules [25], with multiple functional groups, that allow for multivalent drug attachment and a controlled release in a targeted specific way. Despite the many advantages these NPs may offer, there are still some barriers that call for more research, namely at the level of scaling-up their production [25, 26].
- Extracellular vesicles, which are above all, inspired in biological processes, benefiting from essential advantages, such as the inherent high biocompatibility and the reduced immune response it may pose. These properties have drawn high attention over the development of biomolecules nanocarriers based on extracellular vesicles, which have been increasingly scrutinized, especially for cancer therapy, namely in the delivery of nucleic acids [18, 19].

1.1.1.3. Mechanisms of Action of NPs in Therapeutic Contexts

In therapeutic contexts, namely in cancer therapies that use NPs, these can follow different mechanisms of action, which can involve either active (through ligand-receptor interactions) or passive targeting (via the EPR effect) [27, 28]. Being described as an ubiquitous pathophysiological phenomenon, by which certain macromolecular compounds (such as albumin or drugs conjugated with polymers) can progressively accumulate in the vascularized solid tumour area, the EPR effect contributes to the achievement of targeted delivery and retention of anticancer drugs into solid tumours

[29]. Passive targeting relies on the EPR effect, which enables nanoparticles to accumulate in tumour tissue due to the leaky vasculature and poor lymphatic drainage, commonly found in tumours. This phenomenon allows nanoparticles to selectively concentrate in tumour areas more than in healthy tissues. Many studies emphasize the EPR effect as a foundation for passive targeting of tumours by nanoparticles, particularly in polymeric nanoparticle systems [27, 28]. Active targeting involves modifying nanoparticles with ligands that can bind specifically to receptors overexpressed on tumour cells. This ligand-receptor binding facilitates a higher accumulation of nanoparticles directly at the tumour site, enhancing therapeutic effectiveness while minimizing off-target effects. For example, functionalizing nanoparticles with folate or transferrin ligands has shown success in targeting tumours that overexpress corresponding receptors [27].

Polymeric nanoparticles, such as those made from PLGA, are internalized by cells mainly through endocytosis. After cellular uptake, these nanoparticles can be trafficked to endosomes or lysosomes, where they may release their therapeutic payload in response to acidic pH or enzymatic activity. This targeted intracellular release allows for more precise drug action within tumour cells, enhancing efficacy and reducing systemic toxicity. These processes are described in several studies that model nanoparticle uptake and intracellular trafficking, noting that such mechanisms are crucial for the enhanced efficacy of nanoparticle-based drug delivery systems in cancer treatments [28].

1.2. Personalized Therapy in Cancer Treatment

The need for personalized treatment approaches is essentially underscored by the high complexity of cancer and the limitations of conventional therapies. Having available tools such as NPs, which enable targeted delivery of different kinds of molecules, a shift over cancer therapy towards greater specificity is possible, as it is exemplified by PLGA-based ASO treatments that are tailored to enhance chemotherapy precision for breast cancer [27, 28].

1.2.1. Principles of Personalized Therapy

Personalized cancer therapy leverages molecular profiling and biomarker analysis to create treatments uniquely suited to each patient's tumour profile. In breast cancer, molecular markers like human epidermal growth factor receptor 2 (HER2), oestrogen receptor (ER), and progesterone receptor (PR) provide guidance for targeted therapies, enhancing treatment specificity and effectiveness [27]. ASO further support precision

medicine by modulating gene expression related to treatment resistance, such as Clusterin, thereby improving response rates and facilitating a shift toward more personalized oncologic care [28].

1.2.2. Use of Antisense Oligonucleotides (ASO) in Personalized Therapy

ASO are synthetic strands of nucleotides that can specifically bind to messenger RNA (mRNA) sequences, blocking the translation of target genes into proteins. They have emerged as a powerful tool in personalized therapy due to their ability to inhibit the expression of disease-associated genes at the molecular level [30]. In cancer, ASO target genes involved in tumour progression, metastasis, and resistance to chemotherapy, allowing for more precise, patient-specific treatments [31].

ASO are particularly relevant in breast cancer, where they can target overexpressed survival genes like clusterin (*CLU*) [30]. *CLU* gene codifies for CLU, a highly conserved, multifunctional protein with a role in diverse physiological processes such as cell differentiation and morphogenesis, lipid transportation, tissue remodelling and differentiation, as well as cell proliferation, survival and apoptosis [32].
Two sets of different CLU isoforms, secretory and non-secretory, have been described in mammalian cells:
The secretory isoform of CLU (sCLU) is implicated in tumour survival and resistance to conventional treatments. By using ASO to block the expression of sCLU, cancer cells become more susceptible to chemotherapeutic agents [31]. One of the key developments in this area is Custirsen, a second-generation ASO that specifically targets exon 2 of the clusterin gene, leading to the reduction of sCLU expression without affecting the nuclear form of clusterin (nCLU), which has a role in apoptosis induction in healthy cells [32]. Preclinical studies have shown promising results in terms of increasing tumour sensitivity to chemotherapy in various cancers, including breast, prostate, and lung cancer [30].

However, while the potential of ASO in personalized therapy is high, there are significant challenges. These include delivery issues, as ASO need to efficiently penetrate tumour cells, and concerns about off-target effects, which can lead to unintended gene silencing and highlights the need for further clinical validation and refinement of ASO-based treatments [30].

1.2.3. Benefits and Challenges of Personalized Therapy in Breast Cancer

Personalized therapy represents a significant advance in breast cancer treatment, focusing on tailoring treatments to the individual genetic and molecular characteristics of a patient's tumour, which allows for more effective targeting of cancer cells and leads to better treatment outcomes and fewer side effects. The main benefit of personalized therapy lies in its specificity: By targeting genes, proteins, or mutations that are specific to an individual's cancer, these therapies reduce the collateral damage often caused by traditional treatments like chemotherapy and radiation, which can affect healthy cells as well [30].

In breast cancer, personalized therapy often involves targeting hormone receptors (like oestrogen or progesterone receptors in luminal tumours) or HER2 in HER2-positive breast cancer, which benefit significantly from therapies like trastuzumab (Herceptin), which specifically targets the HER2 protein [32].

Despite these benefits, there are considerable challenges associated with personalized therapy in breast cancer mainly due to tumour heterogeneity, where different cells within the same tumour may have distinct genetic profiles, complicating treatment selection [32].

Furthermore, cancer cells can evolve over time, developing resistance to targeted therapies by overexpressing proteins like sCLU, which has been linked to the development of resistance to anticancer treatments like chemotherapy. For this reason, targeting this protein with ASO offers one strategy to overcome this resistance, although delivering these therapies effectively remains a challenge [30].

1.3. Clusterin: Biological Role and Implications in Breast Cancer

Clusterin (CLU) is a glycoprotein with multifunctional roles, implicated in several biological processes related with different hallmarks of cancer including cell survival, apoptosis, tissue remodelling, and protein stabilization [31]. Its involvement in cancer biology has garnered significant attention, particularly due to its dual role in both promoting and inhibiting cell death [31]. Clusterin exists in two main isoforms: the secretory form (sCLU) and the nuclear form (nCLU) [30]. The secretory form, sCLU, functions as an extracellular chaperone, preventing protein aggregation and protecting cells from stress-induced apoptosis. In contrast, nCLU is associated with apoptotic pathways, leading to cell death [30].

In the context of breast cancer, an increased sCLU/nCLU ratio has been linked to increased tumour survival, resistance to chemotherapy, and enhanced metastatic potential, since high levels of sCLU allow cancer cells to avoid programmed cell death, making them more resistant to treatments like chemotherapy and radiation. This survival advantage is particularly evident in aggressive and advanced-stage cancers, reason why sCLU has become a target of interest for therapeutic interventions aimed at increasing tumour sensitivity [31].

1.3.1. Structure and Function of Clusterin

Clusterin is encoded by the *CLU* gene, located on chromosome 8, and exists in various splice variants. These different isoforms result from alternative splicing of the *CLU* gene, leading to the production of both the secretory and nuclear isoforms of the protein.
sCLU, a heavily glycosylated protein, which helps it function as an extracellular chaperone, includes 10 cysteine residues and several glycosylation sites, which are essential for its ability to stabilize misfolded proteins and inhibit their aggregation [30]. sCLU is predominantly found in the extracellular space, where it plays a role in tissue protection, lipid transport, and inhibition of apoptosis.

On the other hand, nCLU, associated with cell death, lacks the glycosylation sites and secretory signal sequence found in sCLU and is primarily located within the nucleus, where it induces apoptosis under stress conditions [32]. This duality in clusterin function, where one isoform promotes cell survival and the other triggers cell death, makes it a particularly interesting target for cancer research [31].
Understanding the mechanisms that regulate the expression of these different isoforms could provide valuable insights into new therapeutic strategies [30].

1.3.2. Aberrant Expression of Clusterin in Cancers

Aberrant expression of clusterin, particularly the overexpression of the sCLU isoform, has been observed in numerous cancer types, including breast, prostate, lung, and ovarian cancers. In breast cancer, sCLU expression increases as the disease progresses from pre-neoplastic stages to primary tumours and metastases and provide cancer cells with a survival advantage by inhibiting apoptosis and promoting resistance to chemotherapy [30]. Studies have shown that sCLU can interfere with the action of pro-apoptotic molecules like tumour necrosis factor (TNF) and Fas, further enhancing the survival of cancer cells [32].

The overexpression of clusterin is not only associated with tumour survival but also with more aggressive tumour behaviour, including enhanced cell migration, invasiveness, and angiogenesis [32]. For instance, sCLU has been shown to correlate with the overexpression of vascular endothelial growth factor (VEGF), a key player in tumour angiogenesis, in primary ovarian carcinomas. This overexpression facilitates the growth of new blood vessels that supply nutrients to the tumour, further promoting its growth and metastasis [30].

1.3.3. Therapeutic Potential of Clusterin Inhibition in Breast Cancer Treatment

Given its role in promoting tumour survival and resistance to therapy, sCLU represents a promising therapeutic target in breast cancer treatment. Inhibition of sCLU using ASO has shown potential in increasing the sensitivity of cancer cells to chemotherapy. Custirsen (OGX-011), an antisense oligonucleotide specifically designed to inhibit sCLU, has demonstrated promising results in preclinical and early clinical trials. By reducing the expression of sCLU, Custirsen enhances the apoptotic effects of chemotherapy, leading to improved treatment outcomes in patients with aggressive cancers [30].

Clinical trials have been conducted to evaluate the efficacy of Custirsen in combination with standard chemotherapeutic agents like docetaxel. In some studies, Custirsen has been shown to reduce tumour progression and improve survival in patients with metastatic prostate cancer and lung cancer [31]. However, results in breast cancer have been more mixed. While Custirsen has been shown to reduce serum clusterin levels and improve treatment response in preclinical models, clinical trials in breast cancer patients have not consistently demonstrated a significant survival benefit probably due to a deficient study design which did not include breast cancer patients with CLU overexpressing tumours. The complexity of tumour biology, including the presence of hormone receptor-positive and triple-negative breast cancer subtypes, may also account for these varying results [30].

Despite these challenges, the inhibition of clusterin remains a promising strategy, particularly for overcoming chemotherapy resistance. As more is learned about the specific mechanisms by which sCLU contributes to tumour survival, future therapies may be able to more precisely target this protein, leading to better outcomes for patients with breast cancer [30, 31, 33, 34].

2. Methodology

2.1. Production of PLGA NPs

2.1.1. Materials and Reagents Used

In the production of PLGA NPs, were used: PLGA (end-capped PLGA with 50:50 D, L-lactide:glycolide ratio and 0.2 Ld g^{-1} inherent viscosity; Purasorb PDLG 5004), acetonitrile (Merck®), 1% (w/v) Poloxamer 407 (Koliphor® p 407, BASF); and ASO's: OGX-011F_2 and OGX-011R_2 (Metabion International AG).

2.1.2. Chemical synthesis of the L-Histidine functionalized targeting polymeric conjugate

2.1.2.1. Functionalization of PLGA-PEG-Histidine

For PLGA-PEG-histidine synthesis were used: a solution of COOH-L-histidine-BOC (COOH-His-BOC; MW ~ 0.255 kDa, 30.6 mg, 120 µmol; Merck®), N-hydroxysuccinimide (41.4 mg, 360 µmol; Merck®) and N,N-dicyclohexylcarbodiimide (74.3 mg, 360 µmol; Merck®) in 9 ml anhydrous dimethylformamide (Merck®) was treated with PLGA-PEG(2K)-NH2 (Mn ~ 17 kDa, 360 mg, 22 µmol; Merck®) and N,N-diisopropylethylamine (37.8 mg, 293 µmol; Merck®) in 5 mL anhydrous dimethylformamide (Merck®). The reaction was stirred for 24 h at room temperature (RT) under inert atmosphere. The resultant mixture was poured into cold diethyl ether (80 mL; Merck®), washed 3x with methanol (40 mL) and dried under vacuum overnight. The polymeric conjugate was re-dissolved and filtered in 15 mL anhydrous dichloromethane (Merck®) and dried under vacuum overnight.

2.1.2.2. Chemical removal of the -BOC protecting group

The Chemical removal of the -BOC protecting group of PLGA-PEG(2K)-His-BOC was perfomed as follow: Trifluoroacetic acid (455 µL, 5.9 mmol) was added to PLGA-PEG(2K)-His-BOC (150 mg, 0.009 mmol) dissolved in anhydrous dichloromethane (16 mL), and the reaction mixture was stirred overnight at RT under inert atmosphere. The reaction mixture was then extracted and neutralized 3x with a 1 M NaOH aqueous solution (8.5 mL). The organic layer was dried under vacuum overnight, washed with cold diethyl ether (10 mL) and dried again.

2.1.3. Procedures for Synthesis of NPs and Encapsulation of ASO

The PLGA NPs were produced using the nanoprecipitation technique, by which NPs are formed in one step [35, 36]. Afterwards, an organic and an aqueous phase were prepared with the purpose to steadily and continuously inject the organic phase into the stirring aqueous solution by using a syringe pump with a 21G needle at a rate of 5 µL/s. The organic phase was obtained by stirring a solution of 250 µL of acetonitrile (Merck®), 9 mg of PLGA, 1 mg of PLGA-PEG-His and the appropriate concentration of each kind of ASO, for approximately 1 h, in a 10 mL glass vial with a cap, to avoid solvent evaporation. The aqueous phase was obtained by preparing 750 µL of 1% (w/v) Poloxamer 407. After injecting the organic phase into the aqueous phase, allowing the formation of PLGA NPs encapsulating the ASO molecules, the NPs solution was left to stir, at RT for at least 1 h, to partially evaporate the organic solvent. Finally, this solution was concentrated in an Amicon filter (Amicon® Ultra 15, 100 k; Merck®) by centrifuging it at 1500 g, until reaching under than 500 µL of concentrated solution of NPs. The latter was resuspended and then, recovered from the Amicon filter by means of a 200 µL pipette, into 1.5 mL microtubes, that were stored at 4º C. This procedure was performed to produce nine different NPs of 3 kinds: i) empty PLGA NPs, to be used as control of the effect of PLGA in cell viability; ii) PLGA NPs encapsulated with OGX-011F_2, an ASO complementary to the clusterin mRNA, reported to inhibit clusterin expression and enhance drug efficacy [37], being the sequence as follows: CAG CAG CAG AGT **C**TT **C**AT CAT; iii) PLGA NPs encapsulated with OGX-011R_2, an ASO non complementary to clusterin mRNA which, when compared to OGX-011F_2, presents 2 mismatches in nucleotide sequence: CAG CAG CAG AGT **A**TT **T**AT CAT. For each kind of oligonucleotide, 4 different concentrations were used: 0.05, 0.2, 0.7 and 2.0 µg/mL.

2.1.4. Characterization of NPs

The mean particle size and surface charge of the nanoparticles (zeta potential) were characterized using a photon correlation spectrophotometer (Malvern Zetasizer Nano ZS). The mean particle size refers to the hydrodynamic diameter, obtained through the

dynamic light scattering (DLS) method, while the surface charge, indicative of the zeta potential, was determined via laser Doppler micro-electrophoresis. All measurements were conducted at a temperature of 25°C, with Milli-Q water as the dispersant. NPs Morphology was evaluated through Transmission Electron Microscopy (TEM) technique, using the Transmission Electron Microscope Jeol JEM 1400. The PLGA NPs sample for TEM technique was prepared as follows: NPs were dispersed in ethanol to avoid aggregation, followed by ultrasonication in order to achieve a homogenous suspension; a copper grid coated with carbon film was prepared, to provide a stable surface for NPs, improving its visibility during TEM analysis and minimizing interference; after ultrasonication, a small drop (5-10µL) of the NPs suspension was placed onto the previously prepared grid, and after a brief settling time, the drop was allowed to air dry, at room temperature, to evaporate the solvent and ensure an evenly deposition of NPs over the grid; afterwards, the grid was ensured to be thoroughly dried, to prevent introduction of artifacts or distortion during TEM analysis.

2.1.5. Evaluation of Encapsulation Efficiency

The efficiency of encapsulation of oligonucleotides was evaluated by measuring the absorbance of each different NP sample in Thermo Scientific NanoDrop™ Spectrophotometer, at wavelength of 260 nm, wavelength at which RNA, ssDNA and dsDNA nucleotides all absorb.

2.2. Cell Culture

2.2.1. Materials Used

Human breast cancer cell lines: MCF7, MDA-MB-231 and SKBR3 were used throughout the work. All these three cell lines were used extensively within the group and were obtained *in house*. Dulbecco's Modified Eagle Medium (DMEM 1x + GlutaMAX™-I, Gibco©) was used as cell culture medium for all the cell lines in study. This medium was supplemented with 10% foetal bovine serum (FBS, Biowest) and 1% penicillin-streptomycin (Pen Strep, Biowest).

For maintaining cell culture procedures, Phosphate-Buffered Saline (PBS 1x; Merck®) was employed as an isotonic solution to preserve osmotic balance. Trypsin (Merck®) was used to dissociate the adherent cell monolayers from both the culture flask bottom and each other, allowing subsequent cell handling and subculturing.

The cytostatics employed in each assay to suppress cell viability, were doxorubicin ($3.44 \cdot 10^{-3}$ M; Eugia Pharma (Malta) Limited), docetaxel ($2.47 \cdot 10^{-2}$ M; Eugia Pharma (Malta) Limited) and paclitaxel ($7.0 \cdot 10^{-3}$ M; TEVA Pharma, S.L.U.), kindly supplied by Marilina García Aranda (Hospital Universitario del Sol, Marbella).

To perform cell viability assays, it was used resazurin (Merck®).

2.2.2. Description of the Cell Lines Used

At the present work, three different breast cancer cell lines were used: MCF7, MDA-MB-231 and SKBR3. The following table resumes the main characteristics of each cell line, which were relevant for this study.

Table 1 - Resume of main characteristics of MCF7, MDA-MB-231 and SKBR3 cell lines (organism and tissue of origin, type of disease, metastatic site from which were isolated, morphology, doubling time [38, 39], CLU expression level [40, 41] – in normalized Transcripts Per Million – and type of cancer).

	Cell Lines		
	MCF7	**MDA-MB-231**	**SKBR3**
Organism	human	human	human
Tissue	breast	breast	breast, mammary gland
Disease	adenocarcinoma	adenocarcinoma	invasive ductal carcinoma
Metastatic Site	pleural effusion	pleural effusion	pleural effusion
Morphology	epithelial-like	epithelial-like	epithelial-like
Doubling Time (h)	24	25	30
CLU Expression Level (nTPM)	664.70	115.80	3887.90
Breast Cancer Type	hormone dependent	triple negative breast cancer	HER2-positive

Since it is of pivotal relevance for the aim of this thesis, the expression level of clusterin in each cell line (measured in nTPM) is highlighted and the comparison between them, is better shown in the graphical representation of Fig. 2.

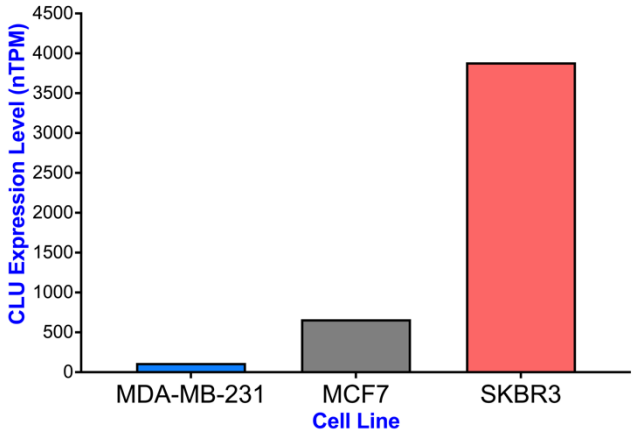

Figure 2 – Graphical representation of CLU expression level in MCF7, MDA-MB-231 and SKBR3 **[38, 39]** (nTPM - normalized Transcripts Per Million).

2.2.3. Experimental Procedures

To each one of the cell lines, it was first confirmed if the PLGA NPs were biocompatible. For this, cytotoxicity of PLGA NPs in all cell lines were evaluated by resazurin assay. Then, it was determined the IC50 of each cytostatic agent used, i.e., the cytostatic agent's concentration that is needed to inhibit cell growth in 50% of the culture. After determination of the IC50 concentrations of doxorubicin (DOX), docetaxel (DTX) and paclitaxel (PTX) for each cell line, cell viability in the presence of the IC50 of each cytostatic agent was evaluated, after treating cells with the different kinds of PLGA NPs. For this, after culturing each one of the cell lines, it was performed a toxicity assay, in which cultured cells were treated with cytostatic agents, followed by a resazurin viability test.

3.2.3.1. Culturing Cell Lines

To maintain cell culture of MCF7, MDA-MB-231 and SKBR3 cells, it was used, as culture medium, DMEM, high glucose, GlutaMAX™-I Supplemented with 10% FBS and 1% Pen Strep. Cells were cultured at 37ºC and 5% CO_2, using T75 flasks. Cells were always kept with a t 80% confluency before being used along the work.

2.2.3.2. Evaluating PLGA NPs Biocompatibility

To evaluate PLGA NPs biocompatibility, each cell line was seeded in 96-well plate, with a density of 19000 cells/well, and incubated at 37ºC and 5% CO_2, for 24h. After this, cell culture medium was removed and replaced by cell culture medium with empty PLGA NPs, in three different dilutions: 1:10, 1:20 and 1:50. For each dilution, were made three replicates. Cells were incubated at 37ºC and 5% CO_2, for 24h. After this period, it was performed a resazurin cell viability test.

2.2.3.3. Cell Viability Test

To determine cell viability, it was performed the resazurin test. The cell culture medium, with each dilution of PLGA NPs, and the negative control (cells untreated with any NPs), were removed and each well was washed thrice with 100 µL of PBS 1x. The PBS 1x was then removed and replaced by cell culture medium with 20% of resazurin. Always protecting resazurin from any light source, the cells were incubated at 37ºC and 5% CO_2, for 3h. After this time of incubation, the content of each 96-well plate was transferred to a black 96-well plate, and the fluorescence was measured in a multi-mode microplate reader (Synergy Mx, BioTek®), at wavelengths of 530 nm (excitation) and 590 nm (emission). The cell viability was calculated by considering negative control as 100% cell viability (cells untreated with PLGA NPs), and the values of fluorescence obtained for the rest of the conditions were calculated in proportion to this, giving the final value of viability for each condition.

2.2.3.4. Cytotoxicity Assay

The cytotoxic agents used were doxorubicin ($3.44 \cdot 10^{-3}$ M), docetaxel ($2.47 \cdot 10^{-2}$ M) and paclitaxel ($7.0 \cdot 10^{-3}$ M). In order to determine the IC50 of each cytotoxic agents, each cell line was seeded in a 96-well plate, with a density of 19000 cells/well. The cells were then incubated at 37ºC and 5% CO_2, for 24h, until reaching confluency. After that, the cell culture medium was removed and replaced with medium with a series of dilutions of each cytotoxic agent (10^{-3} M, 10^{-4} M, 10^{-5} M, 10^{-6} M, 10^{-7} M, 10^{-8} M and 10^{-9} M). Three replicates of each concentration, in each cell line, were performed. Cells were incubated with the cytotoxic agents at 37ºC and 5% CO_2, for 24h and then, it was performed the cell viability assay, as described above. The described procedures were performed in three independent assays (3n), for each cell line.

After calculating the respective IC50 for each cytotoxic agent, these concentrations were used in the following assays to evaluate the cell lines viability in presence of cytotoxic agents, after being treated with PLGA NPs. Therefore, each cell line was seeded in 96-

well plate, using a density of 19000 cells/well, and incubated at 37ºC, 5% CO_2, for 24h, until reaching confluency. After that, cell culture medium was removed from the 96-well plate and replaced for cell culture medium with PLGA NPs: empty PLGA NPs, PLGA NPs encapsulated with 0.05 µg/mL, 0.2 µg/mL, 0.7 µg/mL and 2.0 µg/mL of OGX-011**F**_2 ASO and PLGA NPs encapsulated with 0.05 µg/mL, 0.2 µg/mL, 0.7 µg/mL and 2.0 µg/mL of OGX-011**R**_2 ASO, previously prepared. For each type of NP, three replicates were performed. After the respective addition, cells were incubated at 37ºC, 5% CO_2, for 24h. After this time of incubation of cells with PLGA NPs, the medium with NPs was removed and replaced with cell culture medium with the respective IC50 concentration of doxorubicin, docetaxel and paclitaxel for each cell line, calculated previously. The cells were incubated at 37ºC, 5% CO_2, for 24h were afterwards the resazurin cell viability assay was performed, as described above. This procedure was performed in three independent assays, for each cell line.

2.2.4. Statistical Data Analysis

The data obtained was analysed using Microsoft® Excel. The graphics were plotted using GraphPad Prism10 software.

3. Results and Discussion

3.1. Characterization of PLGA NPs

To better understand the results, it is crucial to characterize physically-chemistry the PLGA NPs produced.

3.1.1. Size, Zeta Potential, Conductivity and Morphology of NPs

The physical-chemistry characterization focused on measuring the mean particle size and the surface charge of the NPs (zeta potential), using a photon correlation spectrophotometer, and evaluating particles morphology, using TEM.

3.1.1.1. Size of NPs

In Table 2 the results of the DLS measurements are shown performed in the 9 samples of PLGA NPs produced and used in biological assays, namely NPs diameter. The results are represented as the mean of NPs diameter (in nm) with the respective standard deviation, averaged from 3 independent measurements.

Table 2 - Size characterization of the 9 PLGA NPs used in biological assays.
Blank – empty PLGA NPs; ctrl – PLGA NPs encapsulated with different concentrations of the ASO OGX_011R_2 (0.05, 0.2, 0.7 and 2.0 µg/mL); CLU-PLGA NPs encapsulated with different concentrations of the ASO OGX_011F_2 (0.05, 0.2, 0.7 and 2.0 µg/mL). In this table, the results are presented as the mean of the size diameter ± standard deviation, which were calculated from 3 independent measurements. N.d. – Not determined.

Sample	Medium	Temperature (ºC)	Size (diameter, nm)					
			1st Peak		2nd Peak		3rd Peak	
			Mean ± SD	%	Mean ± SD	%	Mean ± SD	%
Blank	MiliQ Water	25	212.67 ± 34.64	100	N.d.		N.d.	
ctrl 0.05 µg/mL		25	492.53 ± 23.85	82.63	103.76 ± 16.58	17.37	N.d.	
ctrl 0.2 µg/mL		25	1547.77 ± 924.65	62.37	265.30 ± 164.49	31.93	2696.50 ± 3669.18	8.55
ctrl 0.7 µg/mL		25	757.30 ± 87.85	88.47	93.25 ± 17.40	11.53	N.d.	
ctrl 2.0 µg/mL		25	1655.50 ± 1315.35	59.67	1442.33 ± 1788.25	33.67	2436.60 ± 4003.12	6.63
CLU 0.05 µg/mL		25	360.27 ± 97.23	90.17	43.87 ± 16.35	9.83	N.d.	
CLU 0.2 µg/mL		25	1720.67 ± 361.10	69.63	425.43 ± 116.90	28.70	74.67 ± 0.00	5.00
CLU 0.7 µg/mL		25	639.47 ± 71.43	88.23	85.09 ± 14.50	11.77	N.d.	
CLU 2.0 µg/mL		25	691.03 ± 199.40	93.60	46.67 ± 20.19	6.40	N.d.	

Generally, Table 2 shows 3 peaks of diameter size, representing different size populations of the NPs.

- First peak: represents the main size population of NPs, usually composed of the smallest and most abundant size distribution.
- Second peak: represents a secondary size population of NPs, with much smaller representation, usually constituted of NPs larger in size diameter, most probably due to aggregation during their synthesis and encapsulation of ASO.

- Third peak, when present: refers to the possible existence of larger aggregates or less common NPs sizes that may be also present in suspension, almost negligible.

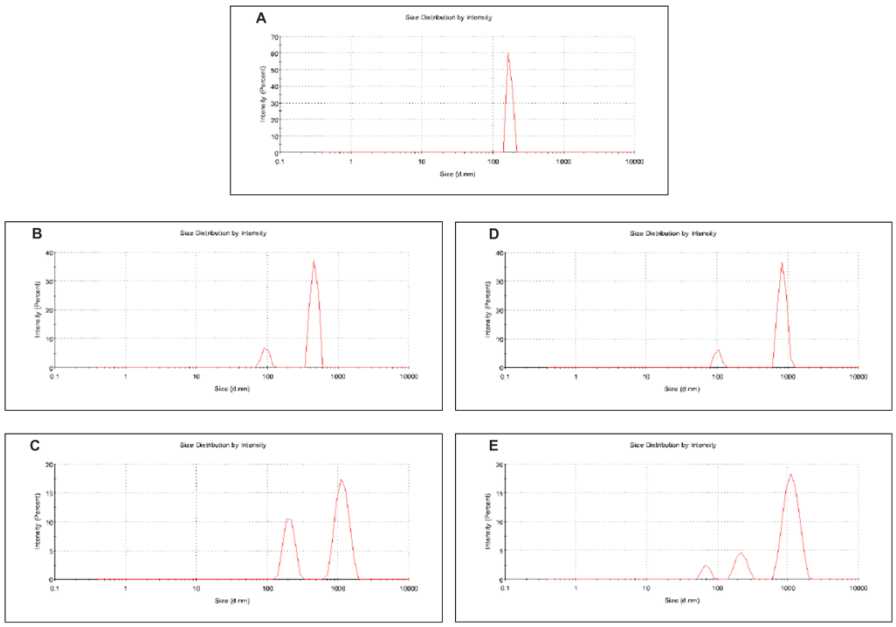

Figure 3 – Graphical representation of NPs sizes, obtained by DLS measurements.
A) Size distribution (nm) by intensity of the blank (empty PLGA NPs). **B** to **E)** Size distribution (nm) of NPs encapsulating different concentrations of the ASO OGX-011**R**_2 (µg/mL): **B**) 0.05; **C**) 0.2; **D**) 0.7; **E**) 2.0.

Blank NPs

The blank, consisting of empty PLGA NPs, without any ASO encapsulated, show high monodispersity, can be observed by the only peak of 212.67 ± 34.64 nm, implying a highly uniform distribution of empty NPs size, which is an important result as a baseline for comparison.

Control NPs

The control NPs, representing PLGA NPs encapsulated with the ASO OGX-011**R**_2, show different sizes according to the ASO concentration. NPs encapsulating 2.0 µg/mL of ASO exhibit a relevant increase of size, when comparing with the blank NPs, showing 3 peaks of NPs diameter size. As the ASO concentration decreases, so does the peak size, presenting the NPs with 0.7 µg/mL and the NPs with 0.05 µg/mL of ASO a first peak size of 757.30 ± 87.85 nm and 492.53 ± 23.85 nm, respectively. However, the NPs encapsulating 0.2 µg/mL of ASO present a much higher first peak size than it would be expected: following the tendency shown, as we were expecting an average size of these NPs between 760 and 490 nm; however, these NPs, besides having three peaks of size, as the 2.0 µg/mL control NPs, show a first peak of 1547.77 ± 924.65 nm. More work should be performed in order to optimize the synthesis of the PLGA NPs when encapsulated with the different ASO OGX-011**R**_2, in terms of polydispersity.

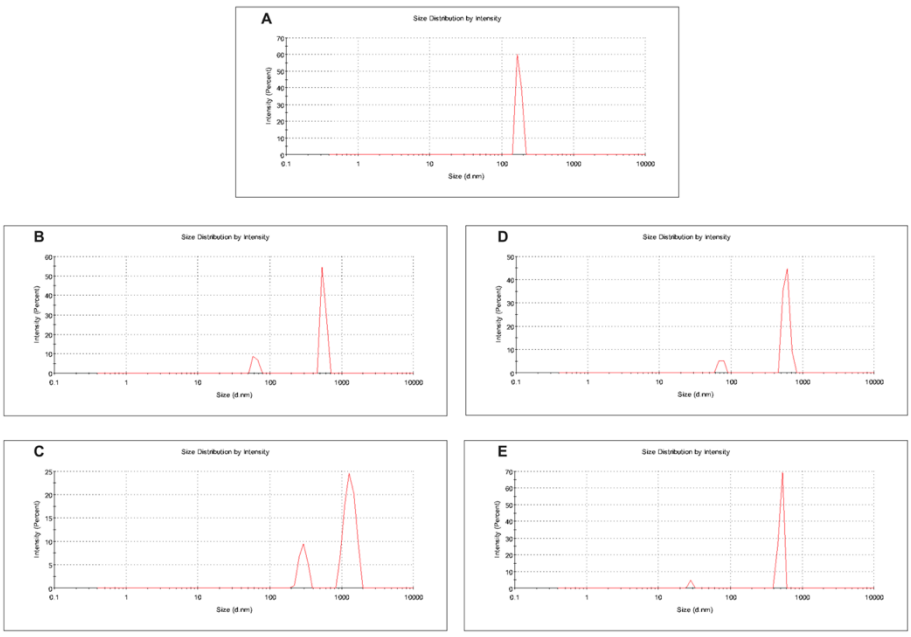

Figure 4 - Graphical representation of NPs sizes, obtained by DLS measurements.
A) size distribution (nm) by intensity of the blank (empty PLGA NPs). **B** to **E)** size distribution (nm) by intensity of NPs encapsulating different concentrations of the ASO OGX-011**F**_2 (µg/mL): **B**) 0.05; **C**) 0.2; **D**) 0.7; **E**) 2.0.

CLU NPs

The CLU NPs, representing PLGA NPs encapsulated with the ASO OGX-011**F**_2, show a similar trend to the one observed previously in the control NPs size. Thus, NPs encapsulating larger concentrations of the ASO show higher diameter sizes than those encapsulating smaller concentrations of the ASO: NPs with 2.0, 0.7 and 0.05 µg/mL

show a first peak size of 691.03 ± 199.40 nm, 639.47 ± 71.43 nm and 360.27 ± 97.23 nm, respectively. However, and similarly to the observations made at the control NPs, 0.2 µg/mL CLU NPs present 3 peaks of size of much higher values than the ones observed at the other ASO concentrations, being the first one of approximately 1720.67 ± 361.10 nm. On other side, the 0.05 µg/mL CLU NPs show the smallest first peak size of all the control and CLU NPs, with no significant secondary peak, depicting a more monodisperse size distribution when compared to higher concentrations of ASO.

Comparing Control and CLU ASO

Analysing Table 2, we can observe that both control (OGX-011**R**_2) and CLU (OGX-011**F**_2) ASO show a tendency to produce larger NPs, when compared to the blank (empty PLGA NPs). It is also observed that higher concentrations of each ASO tend to produce larger NPs, than lower concentrations of the same ASO. However, it is observed that control ASO tend to originate larger NPs than the CLU ASO, when comparing equal concentrations of each. For instance, at concentration 0.7 µg/mL, control ASO originated NPs with a first peak size of 757.30 ± 87.85 nm while the first peak size at CLU ASO verified was of 639.47 ± 71.43 nm. Surprisingly, in both ASO samples, the concentration of 0.2 µg/mL originates NPs with mean particle sizes much higher than it would be expected. Since the experiments were conducted in an independent way, to better understand this fact, it would be necessary to repeat the experiments and evaluate the results, optimizing all the process of synthesis and encapsulation of the different ASO. The appearance of a second and a third peak, which indicates the presence of larger aggregates, is observed at higher concentrations of the ASO, being more pronounced at the control ASO. This fact suggests that OGX-011**R**_2 might induce more aggregation than OGX-011**F**_2. On the other hand, as expected, lower concentrations of the ASO, like 0.05 µg/mL, tend to produce smaller NPs and fewer aggregates, being its first peaks much more pronounced than the second ones observed to each type of sample, suggesting that lower concentrations of the ASO might induce more stable and more monodisperse size distributions of NPs. Nevertheless, even at this lower concentration, a smaller NP size distribution at CLU ASO than at control ASO is observed, being also more pronounced in CLU ASO sample, a more homogenous formulation (since it shows a much stronger first peak, when compared to the second one).

3.1.1.2. Zeta Potential and Conductivity of NPs

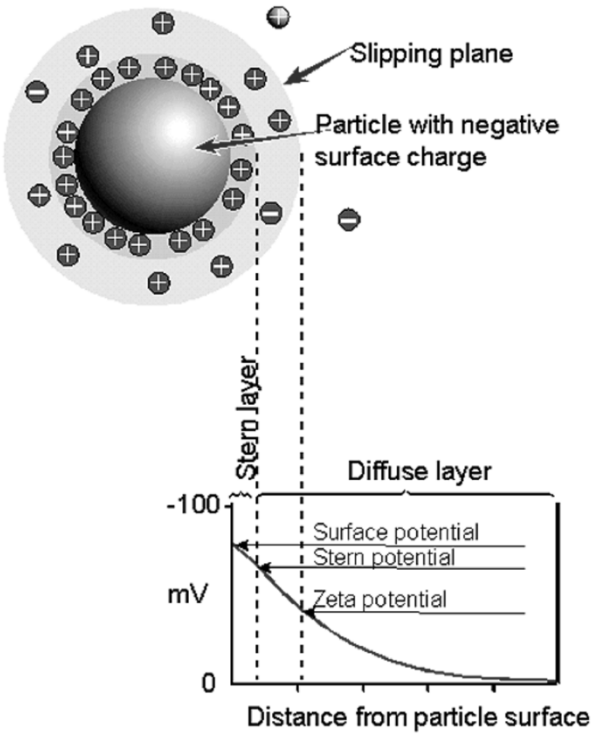

Figure 5 - Schematic representation of zeta potential
(adapted from www.malvern.com).

Upon examining the charge distribution around a charged particle, 2 separate layers can be discerned (electric double layer). The initial layer is the Stern layer, which remains fixed in relation to the particle's surface and possesses an opposing charge [40]. The second component is the mobile diffuse layer. The potential difference between the outer boundary of the Stern layer and the adjacent bulk solution is referred to as the Stern potential. The zeta potential (ζ) denotes the electrokinetic potential established at the interface, or 'slipping plane' between the Stern and diffuse layers of the particle surface [41-44], and is used to assess the stability of colloidal systems, providing information on surface charge [44], that is crucial to determine how NPs interact with biological environments [40], influencing NPs behaviour in drug delivery [44]. Zeta potential plays a pivotal role in stabilizing NPs in nano-drug delivery systems, affecting drug release profiles, targeting, and circulation times in the bloodstream [42], which makes zeta potential a key factor in designing drug delivery systems [40]. A higher absolute zeta potential (either positive or negative) usually indicates a better colloidal stability, since particles repel each other, preventing aggregation. A negative or positive value indicates

the charge direction [44]. It can be measured indirectly using several approaches, covering electroacoustic and electrokinetic methods, optical methods and acoustic methods. Zeta potential is often determined by electrophoresis kinetic method [41], which was the method applied to obtain the results represented at Table 3.

Conductivity indicates how easily electrical current flows through a NP suspension. Conductivity changes can be influenced by the medium, the concentration of NPs, and the ions present. It may be considered as a functional property of NPs that affects their stability, interactions, and performance in diagnostic and therapeutic applications [44, 45], playing a role in determining how NPs behave in suspension, especially in relation to the electric double layer (EDL) that surrounds charged particles which, in turn, influences the overall stability of NP formulations by affecting their zeta potential and mobility in solution [44]. Being generally measured in mS/cm (milisiemens per centimetre), there are some known values of typical suspension's conductivity one can refer to, in order to evaluate the level of conductivity. For instance:

- in pure water, conductivity values are approximately of 0.00005–0.0001 mS/cm, as water is a poor conductor, without ions [46];
- in contrast, sea water (considered as an example of a biological fluid) usually shows conductivity values of 50-55 mS/cm, given its high concentration of ions [46];
- in a nanoparticle suspension, conductivity values will depend upon many factors, such as the type of NPs, their concentration, the nature of dispersion medium, the formation of the EDL, the temperature and the kind of ions present [46, 47]; as an example, studies on silica and titania nanofluids showed a tendency of conductivity increase with the increase of NPs concentration [47].

Thus, values lower than 1 mS/cm indicate poor conduction and are usually found in very dilute or non-ionic systems; a range of values from 1 to 10 mS/cm indicate a moderate conductivity and are typically found in well-dispersed NPs suspensions, suggesting good ion mobility or particle interaction; values higher than 10 mS/cm are considered to indicate high conductivity and are usually found in strong electrolytes or highly charged systems, indicating excellent conduction [46, 47].

Full characterization of zeta potential (in mV) and conductivity (mS/cm), as a mean and a standard deviation, averaged from 3 independent measurements, in 1 independent experiment, are represented in Table 3, for the 9 PLGA NPs in study.

Table 3 - Characterization of zeta potential and conductivity of the 9 PLGA NPs, used in biological assays.
Blank – empty PLGA NPs; ctrl – PLGA NPs encapsulated with different concentrations of the ASO OGX-011**R**_2 (2.0, 0.7, 0.2 and 0.05 µg/mL); CLU - PLGA NPs encapsulated with different concentrations of the ASO OGX-011**F**_2 (2.0, 0.7, 0.2 and 0.05 µg/mL). In this Table, the results are presented as a mean ± standard deviation, which were calculated from 3 independent measurements.

Sample	Medium	Temperature (ºC)	Zeta Potencial (mV)			Conductivity (mS/cm)		
			Mean	±	SD	Mean	±	SD
Blank	MiliQ Water	25	-34.1333	±	5.6048	0.0163	±	0.0071
ctrl 0.05 µg/mL		25	5.6467	±	0.1858	0.0030	±	0.0003
ctrl 0.2 µg/mL		25	11.0000	±	0.4583	0.0103	±	0.0101
ctrl 0.7 µg/mL		25	14.1667	±	0.8622	0.0049	±	0.0003
ctrl 2.0 µg/mL		25	8.7367	±	0.5084	0.0127	±	0.0056
CLU 0.05 µg/mL		25	-1.2867	±	0.2868	0.0075	±	0.0020
CLU 0.2 µg/mL		25	2.5967	±	0.0839	0.0109	±	0.0095
CLU 0.7 µg/mL		25	-12.3333	±	0.3215	0.0093	±	0.0108
CLU 2.0 µg/mL		25	-11.1167	±	1.5861	0.0103	±	0.0092

Zeta Potential Observations

Blank NPs: The blank, consisting of empty PLGA NPs, shows a zeta potential value of -34.1333 mV, indicating a strong negative surface charge, that suggests a good colloidal stability.

Control NPs: Regarding the NPs encapsulating the ASO OGX-011**R**_2, it may be observed that as the concentration of ASO increases, the zeta potential generally moves towards more positive values, meaning a decrease in terms of absolute values, which suggests that the interaction between the ASO and the NP surface, is possibly reducing surface charge stability.

CLU NPs: Contrasting the results observed in control NPs, for CLU samples, which regard NPs encapsulating the ASO OGX-011**F**_2, it may be observed that a higher concentration of the ASO leads to a more negative zeta potential, meaning an increase in terms of absolute values, which indicates a stronger surface charge repulsion and possibly better colloidal stability at higher concentrations. However, there is an exception

in this gradient regarding the concentration of 0.2 µg/mL that shows a zeta potential of 2.5967 mV, contradicting the tendency. Following the trend, a value of approximately -6 mV would be expected and it would be necessary to repeat the experiments and evaluate the results given the inconsistency of the measurements. Nevertheless, in terms of absolute values, we observe a decrease in both control and CLU NPs, when comparing to the blank. A decrease in the absolute zeta potential (less negative) can imply a reduction in surface charge stability, leading to an increase in the polydispersity index and therefore higher aggregation.

Conductivity Observations

Generally, low values of conductivity across the 9 samples were observed, which is typical of MiliQ Water suspensions, a highly purified medium that is known to present very low ionic content [46, 47]. Besides the purity of the suspension medium used, there are some factors that may contribute to the observation of low values of conductivity in the 9 samples, namely:

- The encapsulation of the ASO may be responsible for a decrease in mobility of surface ions or reduction of NPs surface charge, due to the interference that ASO molecules exert in the EDL formation around the NPs, limiting the release of free ions into the medium and leading to less ion exchange between NP surface and solution, thus reducing the overall conductivity [46, 47];
- The NPs concentration in the suspension influences the overall conductivity: lower particle concentration lead to the formation of fewer conductive pathways, typically resulting in lower conductivity [47];
- The type of material used to produce NPs strongly affects the conductivity of suspension; being a biodegradable polymer, PLGA is not a conductive material like metals or metal oxides, as examples, and thus, these NPs themselves do not contribute significantly to the conductivity of the suspensions [46, 47].

Blank NPs: The blank NPs show the highest value of conductivity, of approximately 0.0163 mS/cm, suggesting a more prominent presence of free ions in the blank sample than in the samples of NPs encapsulating ASO, as it would be expected. Without ASO encapsulated, the NP surface may allow more free ions in the suspension medium, increasing the sample conductivity.

Control and CLU NPs: The control NPs and the CLU NPs, besides showing both lower values of conductivity than the blank NPs, show some differences in between:

- in control NPs: a tendency for conductivity increase from lower to higher concentrations of the ASO encapsulated is observed (exception made to the concentration of 0.7 µg/mL, that shows an inconsistent value of 0.0049 mS/cm – the repetition of the experiment would be of the essence to better understand this result); it also shows the second highest value of conductivity among the 9 samples of NPs: at concentration of 2.0 µg/mL, the conductivity is of 0.0127 mS/cm;
- in CLU NPs, the values of conductivity observed at the 4 different concentrations of the CLU ASO are more homogenous than the ones observed in control NPs; nevertheless, lower conductivity at the lowest concentration of ASO is observed, presenting not much higher but more similar values, at the other 3 concentrations; this contrasts with the heterogeneity found among the 4 concentrations of the control ASO, where we can see a more pronounced gradient;
- at lower and comparable concentrations (namely at 0.05 and 0.2 µg/mL), CLU NPs samples show values of conductivity slightly higher than control NPs samples.

Although it is verified that blank NPs show higher conductivity values than NPs encapsulating ASO, that difference is relatively small, suggesting that the encapsulation of the ASO affects ion mobility, but not in a dramatic way. It could mean that the ASO molecule modifies the NPs surface properties without totally neutralizing their conductive potential. Thus, there could still be ion release from the polymer matrix, even though impoverished by the presence of the ASO [46, 47].

Having analysed these parameters – mean particle size, zeta potential and conductivity – it may be said that the encapsulation of the ASO affects both size and the surface charge of the NPs. However, it seems to affect differently the 2 sample types. As mentioned above, the 2 ASO, each composed of 21 nucleotides[1][48], differ only in 2 mismatches:

[1] The ASO are composed of unitary components, designated as nucleotides, made up of a nitrogenous base, a phosphate group, and a sugar molecule. Nucleotides are named after the nitrogenous bases of 4 kinds: adenine (A), guanine (G), cytosine (C) and thymine (T). These nitrogenous bases are chemically different: A and G are purines, C and T are pyrimidines.

OGX-011**F**_2: CAG CAG CAG AGT **C**TT **C**AT CAT

OGX-011**R**_2: CAG CAG CAG AGT **A**TT **T**AT CAT

As can be seen, the 2 mismatches, in the kind of C-A and C-T, are separated by 2 nucleotides, being the C-A mismatch closer to the centre of the ASO and the C-T, closer to its end. This fact could be of relevance, when trying to understand the different behaviour of the NPs, in terms of mean particle size and of zeta potential. The way in which these mismatches can interfere both in mean particle size and zeta potential, has been widely studied. The encapsulation of ASO, or of any nucleic acids, can influence the NPs surface charge, and consequently, its zeta potential, given their negative charge from the phosphate backbone [49]. Even minor structural changes, such as 2 nucleotide mismatches, can have profound impact on the way in which ASO specifically bind to the polymer or functional groups on the NPs surface, affecting colloidal stability [50]. Furthermore, these mismatches might have influence on the ASO' secondary structure or on their interaction with the nanocarrier, influencing their spatial conformation and altering how they fit or embed within the NP matrix, which can affect the compactness and overall NPs size, potentially causing differences in NP aggregation and electrostatic interactions, which are directly linked to changes in size and zeta potential [49, 50]. Several factors, such as the nature of the base pairs and the position within the ASO sequence, are responsible for the magnitude of impact that these mismatches exert over ASO properties. A mismatch that involves purines contributes to a higher disruption of the ASO secondary structure than it does a mismatch of the kind purine-pyrimidine, leading to more pronounced alterations in zeta potential and particle size [50]. Mismatches of the nature G-T and A-C, which result in weaker hydrogen bonding, have been shown to be more destabilizing, influencing ASO binding to charged polymers or NPs components, potentially leading to larger changes in NPs behaviour [49, 50]. Central mismatches have a more pronounced impact than terminal mismatches at 5' or 3' ends, since they significantly disrupt stability and binding, affecting interactions with NPs. Although terminal mismatches have shown lesser impact on ASO structural stability, they still influence NPs properties, especially regarding the way in which the ASO anchor or are exposed to the NP [49, 50]. Moreover, central (C-A) and terminal (C-T) mismatches, especially when in close proximity, substantially undermine the ASO structure: while C-A tends to cause a considerable structural distortion, originating a more flexible conformation of the ASO, the nearby C-T compounds this effect. This structural instability leads to an increase in NPs size, given the lesser compactness of the ASO, possibly

disrupting surface uniformity and altering zeta potential by exposing more of the phosphate backbone, which reduces NPs stability and efficacy [49, 50]. Therefore, this combination of mismatches may diminish gene silencing efficiency (which is the aim of having a control ASO), but it may pose challenges in NPs production.

3.1.1.3. Morphology of NPs

In order to characterize the PLGA NPs morphology, we used transmission electron microscopy technique, applied to samples of empty PLGA NPs. In Fig. an image of the empty NPs produced, obtained by TEM, is presented.

The TEM image, taken at a magnification of 100,000 x, with a scale bar of 100 nm, shows that the PLGA NPs are well-dispersed, with no aggregates, presenting a shape homogenously spherical, and with diameters ranging from 20 to 50 nm, all of which reveals monodispersity. The size exhibited at the image does not match the sizes found with DLS technique and that is probably due to the processes involved in the NPs sample preparation for TEM, which comprises, for instance, drying of the sample, contrasting the conditions found to measurement by DLS, where the NPs sample corresponds to a suspension of PLGA NPs in MiliQ water. The high contrast between the NPs and the surrounding background, indicates that the NPs present a strong electron density.

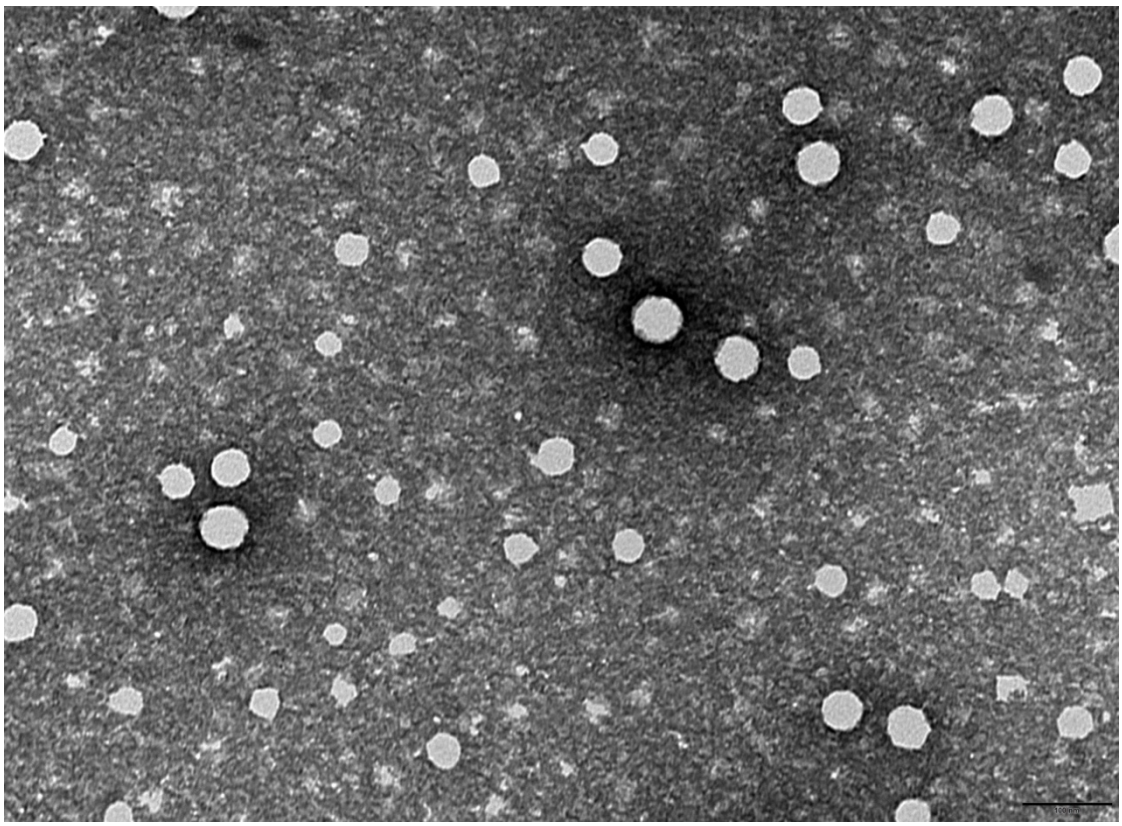

Figure 6 - Transmission electron microscopy (TEM) image of PLGA nanoparticles (NPs).

The NPs diameters exhibited range from 30 to 50 nm. They are well-dispersed, showing no aggregates. The NPs also show a strong electron contrast, possibly due to their inherent density. The image at a magnification of 100,000 times (scale bar = 100 nm).

3.1.2. Encapsulation Efficiency of ASO

Although we performed an encapsulation efficiency evaluation of the 8 types of ASO-loaded NPs with NanoDrop™, as referred before, the results were inconclusive, most probably due to the highly concentrated suspension medium. A repetition of the procedures of measurement with NanoDrop™ would be needed, which was not possible yet due to lack of time.

3.2. Effects of PLGA NPs on Breast Cancer Cell Lines

3.2.1. Cell Viability Analysis

Here are presented the results of the different viability tests performed.

3.2.1.1. Biocompatibility of PLGA with Cell Lines

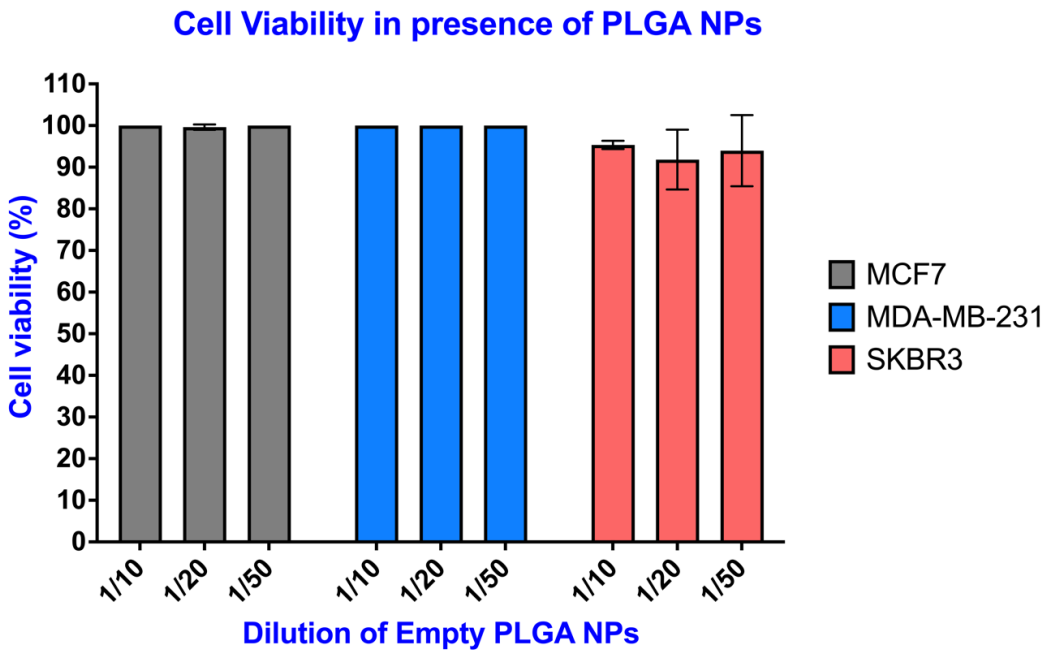

Figure 7 - Graphical representation of cell viability of the cell lines MCF7, MDA-MB-231 and SKBR3, after treatment with empty PLGA NPs. Each cell line was treated with 3 different dilutions of PLGA NPs suspensions: 1/10, 1/20 and 1/50.

The results of cell viability of the different breast cancer cell lines used in this study – MCF7, MDA-MB-231 and SKBR3 – after being treated with empty PLGA NPs are represented in Fig. 4. To further understand each cell line viability in the presence of the polymer PLGA, 3 different dilutions of the suspension of NPs were tested: 1:10, 1:20 and 1:50. Comparing the 3 cell lines, the results of cell viability are very similar. We may observe that cell viability in all cell lines is consistently high, throughout the different dilutions, exhibiting values invariably next to 100%.

The high cell viability values observed, across the 3 different dilutions, suggest that empty PLGA NPs are not cytotoxic to the tested cell lines, indicating biocompatibility of PLGA NPs, which is a crucial feature when considering its use as a gene delivery vector. Most importantly, this lack of significant reduction of viability among the 3 different subtypes of breast cancer cell lines, including the oestrogen receptor-positive (MCF7), the HER2-positive (SKBR3) and the triple-negative (MDA-MB-231), emphasize their safety in this *in vitro* context. Given these results, it is safe to say that PLGA NPs can provide a stable platform for further functionalization, such as the loading of ASO molecules, and supports its future use for therapeutic applications in breast cancer, since the system reveals to be itself non-toxic. In addition, the consistency of cell viability response across the 3 different cell lines, each one representing a different subtype of breast cancer, suggests that PLGA NPs have a broad spectrum of safe applications in this disease. This point is of relevant consideration in a future context of translating this system to a clinical approach. The scientific literature widely reports the minimal cytotoxicity and high biocompatibility of PLGA NPs in cancer cell or other cell types [20, 21, 51].

3.2.1.2. Calculation of IC50

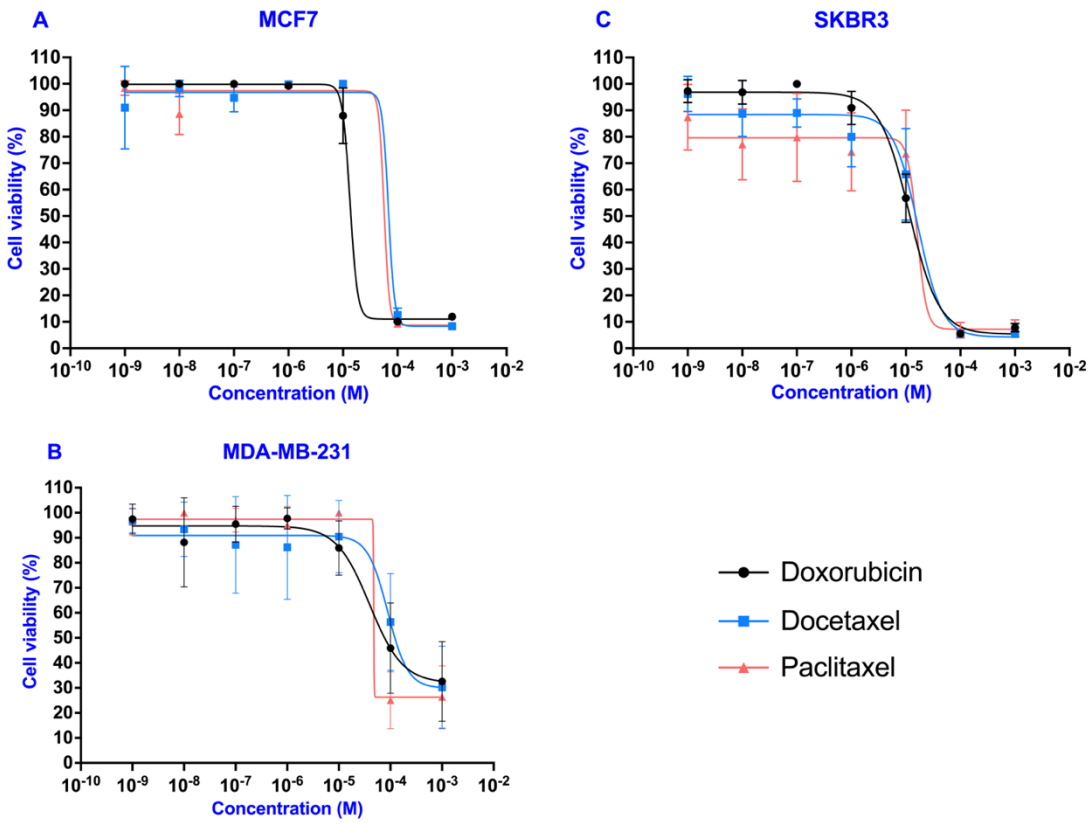

Figure 8 - Graphical representation of the curve of dose-response of each cell line to the cytotoxic agents in study (doxorubicin, docetaxel and paclitaxel). A) MCF7; **B)** MDA-MB-231; **C)** SKBR3. The values were obtained from 3 measurements of each cytotoxic agent, for each cell line, obtained from 3 independent assays.

The main objective of this part of the work was to analyse the sensitivity of the 3 different breast cancer cell lines (MCF7, MDA-MB-231 and SKBR3) to the effects of the cytostatic agents in study (DOX, DTX and PTX), and to determine the half maximal inhibitory concentration (IC50) for each one of the 3 drugs. In Fig. 8 the curves of dose-response of each cell line are represented. In response to increasing concentrations of each one of the cytostatic agents (from 10^{-9} M to 10^{-3} M), all 3 cell lines presented a dose-response decrease in cell viability. Generally, MCF7 (Fig. 8A) and SKBR3 (Fig. 8C) exhibit a sharper decline in cell viability at lower concentrations, especially for DOX and PTX, suggesting a higher sensitivity to these agents, while for MDA-MB-231 (Fig. 5B), this decline appeared to be at slightly higher concentrations, indicating this cell line as more resistant to the agents than the 2 others. Nevertheless, the IC50 values for each cytostatic agent differed across the three cell lines, as it is represented in Table 4.

Table 4 - IC50 values (in M) for the three cytostatic agents, in each one of the three cell lines.

	Cytostatic agent IC50:		
	Doxorubicin	**Docetaxel**	**Paclitaxel**
MCF7	10^{-5}	$4.5 \cdot 10^{-5}$	$3.5 \cdot 10^{-5}$
MDA-MB-231	$5 \cdot 10^{-5}$	$8 \cdot 10^{-5}$	$5 \cdot 10^{-5}$
SKBR3	$3 \cdot 10^{-5}$	$5 \cdot 10^{-5}$	$5 \cdot 10^{-5}$

MCF7 cells showed the lowest IC50 for DOX, suggesting this cell line as the most sensitive to this cytostatic agent. As for MDA-MB-231, it presented the highest IC50 across the 3 agents, exception made for PTX, in which the IC50 value is higher than the one exhibited by MCF7 cells, but equal to the one showed by SKBR3 cells; nevertheless, this could be suggestive of a more resistant phenotype, when regarding MDA-MB-231 cells.

The variations observed in cytostatic agents' sensitivity may be due to the different molecular attributes of each cell line. For instance, MCF7 cells, characterized as oestrogen receptor-positive (ER+), exhibit a favourable response to anthracyclines like DOX, which may account for their heightened sensitivity to this agent. This is supported by Howard *et al.* (2022) in a study that also presents mathematical models describing the dynamics of drug-sensitive and resistant cell populations in MCF7 [52]. There are additional findings, namely by Xu *et al.* (2014) and Christowitz *et al*. (2019), that support the idea of MCF7 cells accumulating DOX more effectively, explaining its increased sensitivity to this agent [53, 54]. MDA-MB-231 cells, characterized as triple-negative and more aggressive, have been documented, for instance by Xu *et al.* (2014) and Christowitz *et al.* (2019), as more resistant to chemotherapeutic agents [53, 54], which is consistent with the IC50 values here presented. Regarding SKBR3 cell line, there are studies that show a correlation between HER2 overexpression and higher sensitivity to taxane-based drugs, like PTX [54].

3.2.1.3. Cell Viability After Treatment with Loaded PLGA NPs

After being incubated with PLGA NPs loaded with four different concentrations (0.05 µg/mL, 0.2 µg/mL, 0.7 µg/mL and 2.0 µg/mL) of the two ASO (control, OGX-011**R**_2, and CLU, OGX-011**F**_2), the three cell lines were treated with the respective IC50 of each cytostatic agent. The viability of each cell line was then evaluated, and its results are represented in Fig. 6; each graphic refers to one of the different ASO' concentrations, being represented in the X axis, the type of PLGA NP used (control or CLU) combined with the following kind of cytostatic treatment (doxorubicin – DOX, docetaxel – DTX, or paclitaxel – PTX).

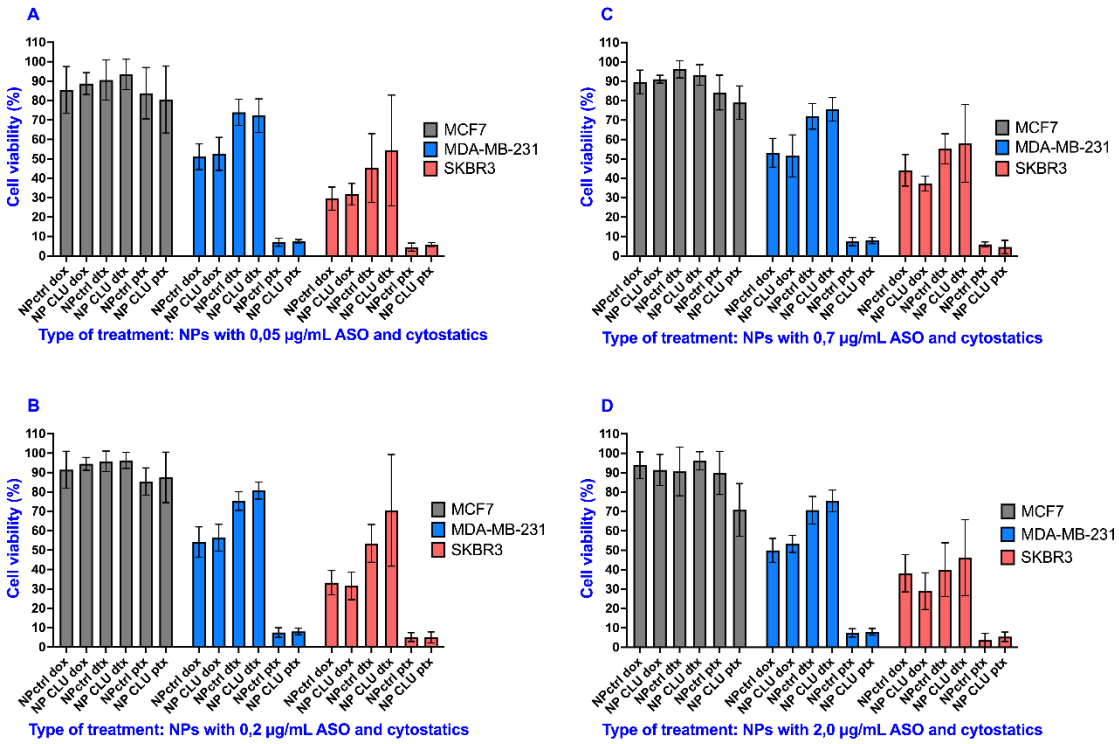

Figure 9 - Graphical representation of cell viability of MCF7, MDA-MB-231 and SKBR3, after treatment with NPs loaded with ASO followed by treatment with the IC50 concentration of doxorubicin (DOX), docetaxel (DTX) and paclitaxel (PTX) for each cell line. In each graphic, in the X axis is represented the type of NP used (ctrl or CLU) combined with the following treatment of each cytotoxic agent (DOX, DTX, PTX): NP ctrl – PLGA NPs loaded with OGX-011**R**_2; NP CLU – PLGA NPs loaded with OGX-011**F**_2. The concentration of each ASO used in NPs (µg/mL): **A)** 0.05; **B)** 0.2; **C)** 0.7; **D)** 2.0.

After being incubated with PLGA NPs loaded with 4 different concentrations (0.05, 0.2, 0.7 and 2.0 µg/mL) of the 2 ASO (control, OGX-011**R**_2, and CLU, OGX-011**F**_2), the 3 cell lines were treated with the respective IC50 of each cytostatic agent. The viability of each cell line was then evaluated, and its results are represented in Fig. 9; each graphic refers to one of the different ASO concentrations, being represented in the X axis, the

type of PLGA NP used (control or CLU) combined with the following type of cytostatic treatment (DOX, DTX, or PTX).

Analysing the 4 graphs (Figs. 9A-D), results suggest that MCF7 generally shows a higher viability, when compared to MDA-MB-231 and SKBR3, after treatment with the cytostatic agents, indicating that these last 2 cell lines are more sensitive to these NPs treatments, using the tested concentrations (especially at higher ASO concentrations). A general trend of decreasing cell viability can be observed across the 4 graphs, as the ASO concentration increases. Although this trend is applied to all cell lines, it is more pronounced in MDA-MB-231 and SKBR3, showing the latter the strongest decrease. This could be indicative of a dose-dependent cytotoxic effect of the NPs loaded with ASO. It is also observed a sharper reduction in viability of MDA-MB-231 and SKBR3 at the highest concentration (2.0 µg/mL), indicating that the combination of ASO and cytostatic agent could be more effective at higher concentrations. However, some limitations must be considered when interpreting these findings. Firstly, we did not measure CLU mRNA or protein levels, before and after ASO treatment, making it challenging to confirm that the observed effects directly result from CLU silencing. Additionally, NP internalisation by the cells was not assessed, leaving the precise intracellular availability of ASO unknown. Lastly, we did not compare the effects of encapsulated versus naked ASO, so it remains unclear if encapsulation grants any specific benefits in delivery efficiency or therapeutic efficacy. Addressing these aspects in future work would provide a more comprehensive understanding of the mechanisms underlying these observations.

The effectiveness of the different treatments appears to vary specifically through cell lines. To better visualize this, in Fig. 10 the same data of the assay mentioned above, was used to plot three graphs that emphasize the role of each cytostatic agent across the different cell lines, showing a different perspective. As we can see, MCF7 show high viability values for all treatments, across the different concentrations of ASO; SKBR3 cells (HER2-positive) and MDA-MB-231 cells (TNBC) seem to be more sensitive to these treatments, since they show consistently lower viability values in the presence of ASO-loaded NPs with every cytostatic agent in study, especially in combination of NPs with PTX. This reduction of viability is more pronounced in SKBR3, indicating these cells as more susceptible to the combined treatment here studied.

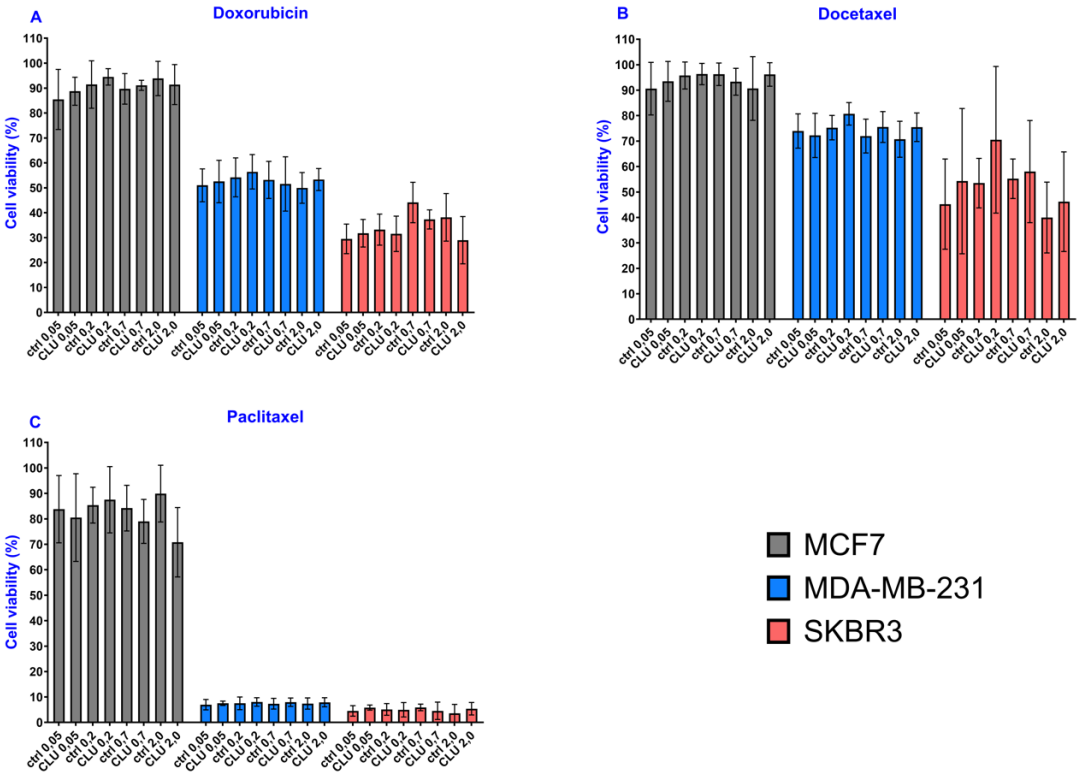

Figure 10 - Graphical representation of cell viability of MCF7, MDA-MB-231 and SKBR3, after treatment with NPs loaded with ASO followed by treatment with the IC50 concentration of doxorubicin, docetaxel and paclitaxel for each cell line, in the perspective of each cytostatic agent. In each graphic, in the X axis is represented the type of NP used (ctrl or CLU) followed by the ASO' concentration loaded in NPs: ctrl – PLGA NPs loaded with OGX-011**R**_2; CLU – PLGA NPs loaded with OGX-011**F**_2; 0.05 – concentration of ASO used in NPs equal to 0,05 µg/mL; 0.2 – concentration of ASO used in NPs equal to 0,2 µg/mL; 0.7 – concentration of ASO used in NPs equal to 0,7 µg/mL; 2.0 – concentration of ASO used in NPs equal to 2,0 µg/mL. Each graph represents the results of one cytostatic agent: A – doxorubicin; B – docetaxel; C – paclitaxel.

3.2.2. Comparison Between Cell Lines

To better understand these differences in cell viability results and determine if they are simply due to random variations or, on the contrary, if there is statistical evidence that supports the hypothesis that delivering ASO to breast cancer cells increases its sensitivity to conventional chemotherapeutic drugs (DOX, DTX and PTX), the p-value was calculated between cell viability results. In order to do so, cell viability results were processed, using the values of the control (cells treated only with cytostatic agents), CLU NPs (cells previously incubated with PLGA NPs loaded with ASO OGX-011**F**_2 and treated with cytostatic agents) and control NPs (cells previously incubated with PLGA NPs loaded with ASO OGX-011**R**_2 and treated with cytostatic agents). The p-value was calculated between the experimental conditions control *vs* CLU NPs and CLU NPs *vs* control NPs, for each concentration of the encapsulated ASO (0.05, 0.2, 0.7 and 2.0

µg/mL) in every treatment with cytostatic drugs (DOX, DTX and PTX). The results of these data processing are shown in the following Tables: Table 5 refers to MCF7 results; Table 6 refers to MDA-MB-231 results and Table 7 refers to SKBR3 results. In each Table, p-values inferior to 0.05 are highlighted.

Table 5 - Comparison of cell viability results of MCF7 cell line, in 3 different experimental conditions. For the viability tests, cells were cultured in 3 different conditions: cells without pre-treatment with NPs and treated only with cytostatic agent (control); cells submitted to a pre-treatment with NPs control (PLGA NPs loaded with ASO OGX-011**R**_2) followed by the cytostatic agent treatment ($NP_{Control}$); cells submitted to a pre-treatment with NPs CLU (PLGA NPs loaded with ASO OGX-011**F**_2) followed by the cytostatic agent treatment (NP_{CLU}). For each type of NP, 4 different concentrations of loaded ASO were used: 0.05, 0.2, 0.7 and 2.0 µg/mL. The cell viability results are presented as the mean ± standard deviation and were obtained from 3 measurements of 2 independent assays. The differences of cell viability results between the 3 different experimental conditions, were assessed by calculating the p-value: highlighted values refer to differences statistically significant or not due just by random variation (where $p<0.05$).

MCF7		Doxorubicin		Docetaxel		Paclitaxel	
		Mean ± SD	p-value	Mean ± SD	p-value	Mean ± SD	p-value
0,05 µg/mL	Control	95.53 ± 4.99	0.0516	95.79 ± 12.24	0.4662	70.79 ± 10.91	0.2532
	NP_{CLU}	88.74 ± 5.63		103.39 ± 21.31		81.52 ± 18.73	
	$NP_{Control}$	88.07 ± 16.44	0.9261	96.58 ± 17.06	0.5548	85.61 ± 16.28	0.6948
	NP_{CLU}	88.74 ± 5.63		103.39 ± 21.31		81.52 ± 18.73	
0,2 µg/mL	Control	95.53 ± 4.99	0.6843	95.79 ± 12.24	0.2681	70.79 ± 10.91	**0.0367**
	NP_{CLU}	94.50 ± 3.31		106.12 ± 17.79		87.50 ± 13.03	
	$NP_{Control}$	98.22 ± 16.89	0.6080	103.77 ± 14.13	0.8049	85.00 ± 7.04	0.7348
	NP_{CLU}	94.50 ± 3.31		106.12 ± 17.79		87.50 ± 13.03	
0,7 µg/mL	Control	95.53 ± 4.98	0.0727	95.79 ± 12.24	0.5645	70.79 ± 10.91	0.1782
	NP_{CLU}	91.12 ± 2.03		100.88 ± 16.96		79.02 ± 8.63	
	$NP_{Control}$	91.06 ± 9.05	0.9880	101.41 ± 11.10	0.9498	84.22 ± 8.96	0.3299
	NP_{CLU}	91.12 ± 2.03		100.88 ± 16.96		79.02 ± 8.63	
2,0 µg/mL	Control	95.53 ± 4.98	0.3125	95.79 ± 12.24	0.3196	70.79 ± 10.91	0.9978
	NP_{CLU}	91.42 ± 8.04		104.33 ± 15.78		70.81 ± 13.61	
	$NP_{Control}$	97.68 ± 11.14	0.2902	93.88 ± 16.03	0.2819	90.84 ± 12.14	**0.0227**
	NP_{CLU}	91.42 ± 8.04		104.33 ± 15.78		70.81 ± 13.61	

As we can see in Table 5, generally for MCF7 cells there were no significant differences between the experimental conditions tested. Nevertheless, there are 2 results that draw are noteworthy: there is statistical evidence at ASO concentration of 0.2 µg/mL between control and NP_{CLU}, and between NP_{CLU} and $NP_{Control}$, both under the effect of PTX. However, the first situation is irrelevant, since cell viability of NP_{CLU} is even higher than that of control; as for the second situation, there is in fact statistical evidence for 2.0

µg/mL NP_{CLU} combined with PTX, but it is not conclusive, since the cell viability of the control for the same conditions is very similar to the value observed at NP_{CLU}. These results suggest that, for these concentrations, CLU ASO appears not to have a relevant influence in sensitizing MCF7 cells to conventional chemotherapeutic agents.

Table 6 - Comparison of cell viability results of MDA-MB-231 cell line, in 3 different experimental conditions. For the viability tests, cells were cultured in 3 different conditions: cells without pre-treatment with NPs and treated only with cytostatic agent (control); cells submitted to a pre-treatment with NPs control (PLGA NPs loaded with ASO OGX-011**R**_2) followed by the cytostatic agent treatment ($NP_{Control}$); cells submitted to a pre-treatment with NPs CLU (PLGA NPs loaded with ASO OGX-011**F**_2) followed by the cytostatic agent treatment (NP_{CLU}). For each type of NP, 4 different concentrations of loaded ASO were used: 0.05, 0.2, 0.7 and 2.0 µg/mL. The cell viability results are presented as the mean ± standard deviation and were obtained from 3 measurements of 2 independent assays. The differences of cell viability results between the 3 different experimental conditions, were assessed by calculating the p-value: differences statistically significant or not due just by random variation (where $p<0.05$), were not found for this cell line.

MDA-MB-231		Doxorubicin		Docetaxel		Paclitaxel	
		Mean ± SD	p-value	Mean ± SD	p-value	Mean ± SD	p-value
0,05 µg/mL	Control	52.37 ± 11.11	0.9776	77.49 ± 6.49	0.2604	8.68 ± 1.71	0.1756
	NP_{CLU}	52.53 ± 8.51		72.21 ± 8.68		7.54 ± 0.87	
	$NP_{Control}$	51.01 ± 6.59	0.7373	73.96 ± 6.73	0.7053	7.00 ± 2.04	0.5641
	NP_{CLU}	52.53 ± 8.51		72.21 ± 8.68		7.54 ± 0.87	
0,2 µg/mL	Control	52.37 ± 11.11	0.4638	77.49 ± 6.49	0.3416	8.68 ± 1.71	0.5401
	NP_{CLU}	56.43 ± 6.88		80.69 ± 4.42		8.06 ± 1.66	
	$NP_{Control}$	54.20 ± 7.80	0.6103	75.27 ± 4.82	0.0698	7.53 ± 2.48	0.6706
	NP_{CLU}	56.43 ± 6.88		80.69 ± 4.42		8.06 ± 1.66	
0,7 µg/mL	Control	52.37 ± 11.11	0.8994	77.49 ± 6.49	0.6003	8.68 ± 1.71	0.4838
	NP_{CLU}	51.54 ± 10.88		75.53 ± 6.05		7.97 ± 1.66	
	$NP_{Control}$	53.18 ± 7.43	0.7668	71.96 ± 6.63	0.3523	7.38 ± 2.08	0.5974
	NP_{CLU}	51.54 ± 10.88		75.53 ± 6.05		7.97 ± 1.66	
2,0 µg/mL	Control	52.37 ± 11.11	0.8464	77.49 ± 6.49	0.5697	8.68 ± 1.71	0.4873
	NP_{CLU}	53.34 ± 4.40		75.43 ± 5.59		7.95 ± 1.78	
	$NP_{Control}$	49.98 ± 6.16	0.3026	70.71 ± 7.08	0.2290	7.44 ± 2.20	0.6643
	NP_{CLU}	53.34 ± 4.40		75.43 ± 5.59		7.95 ± 1.78	

For MDA-MB-231 cells, as can be seen in from Table 6, no statistical evidence that NP_{CLU} significantly enhances the cytotoxicity of DOX, DTX, or PTX was observed. in all ASO concentrations and in every treatment condition, there was no statistically significant reduction in cell viability when comparing control to NP_{CLU} or $NP_{Control}$ to NP_{CLU}. Also, these results suggest that, for these concentrations, CLU ASO appears not to have a relevant influence in sensitizing MDA-MB-231 cells to conventional chemotherapeutic agents.

Table 7 - Comparison of cell viability results of SKBR3 cell line, in 3 different experimental conditions. For the viability tests, cells were cultured in 3 different conditions: cells without pre-treatment with NPs and treated only with cytostatic agent (control); cells submitted to a pre-treatment with NPs control (PLGA NPs loaded with ASO OGX-011**R**_2) followed by the cytostatic agent treatment ($NP_{Control}$); cells submitted to a pre-treatment with NPs CLU (PLGA NPs loaded with ASO OGX-011**F**_2) followed by the cytostatic agent treatment (NP_{CLU}). For each type of NP, 4 different concentrations of loaded ASO were used: 0.05, 0.2, 0.7 and 2.0 µg/mL. The cell viability results are presented as the mean ± standard deviation and were obtained from 3 measurements of 2 independent assays. The differences of cell viability results between the 3 different experimental conditions, were assessed by calculating the p-value: highlighted values refer to differences statistically significant or not due just by random variation (where $p<0.05$).

SKBR3		Doxorubicin		Docetaxel		Paclitaxel	
		Mean ± SD	p-value	Mean ± SD	p-value	Mean ± SD	p-value
0,05 µg/mL	Control	43.35 ± 3.22	**0.0013**	60.57 ± 18.44	0.6596	6.98 ± 1.53	0.1625
	NP_{CLU}	31.78 ± 5.55		54.27 ± 28.52		5.86 ± 0.99	
	$NP_{Control}$	29.52 ± 5.92	0.5102	45.24 ± 17.70	0.5247	4.57 ± 2.06	0.1970
	NP_{CLU}	31.78 ± 5.55		54.27 ± 28.52		5.86 ± 0.99	
0,2 µg/mL	Control	43.35 ± 3.22	**0.0041**	60.57 ± 18.44	0.4377	6.98 ± 1.53	0.1625
	NP_{CLU}	31.56 ± 7.10		72.59 ± 31.42		4.99 ± 2.84	
	$NP_{Control}$	33.22 ± 6.23	0.6758	53.48 ± 9.72	0.1852	5.14 ± 2.28	0.9250
	NP_{CLU}	31.56 ± 7.10		72.59 ± 31.42		4.99 ± 2.84	
0,7 µg/mL	Control	43.35 ± 3.22	**0.0147**	60.57 ± 18.44	0.8224	6.98 ± 1.53	0.1493
	NP_{CLU}	37.33 ± 3.84		58.00 ± 20.06		4.58 ± 3.43	
	$NP_{Control}$	44.12 ± 8.11	0.0932	55.21 ± 7.76	0.7569	5.91 ± 1.29	0.3949
	NP_{CLU}	37.32 ± 3.84		58.00 ± 20.06		4.58 ± 3.43	
2,0 µg/mL	Control	43.35 ± 3.22	**0.0056**	60.57 ± 18.44	0.2198	6.98 ± 1.53	0.2160
	NP_{CLU}	28.99 ± 9.46		46.20 ± 19.56		5.42 ± 2.46	
	$NP_{Control}$	38.16 ± 9.55	0.1258	39.98 ± 13.91	0.5399	3.64 ± 3.48	0.3304
	NP_{CLU}	28.99 ± 9.46		46.20 ± 19.56		5.42 ± 2.46	

Regarding SKBR3 cells, and as can be seen in Table 7, statistical significance is observed when comparing cell viability values of control group to the ones observed at NP_{CLU} group, in every ASO concentration, for treatment with DOX. However, these results are not supported by the differences between the groups $NP_{Control}$ and NP_{CLU}, which are not statistically significant, within the same treatment. On treatments with DTX or with PTX, no statistically significant difference is observed in cell viability when comparing control to NP_{CLU} or $NP_{Control}$ to NP_{CLU}, in any of the ASO concentrations. Therefore, these results suggest that, for these concentrations, CLU ASO appears not to have a relevant influence in sensitizing SKBR3 cells to conventional chemotherapeutic agents.

3.2.3. Impact of CLU loaded nanoparticles on cell sensitivity to chemotherapeutic agents

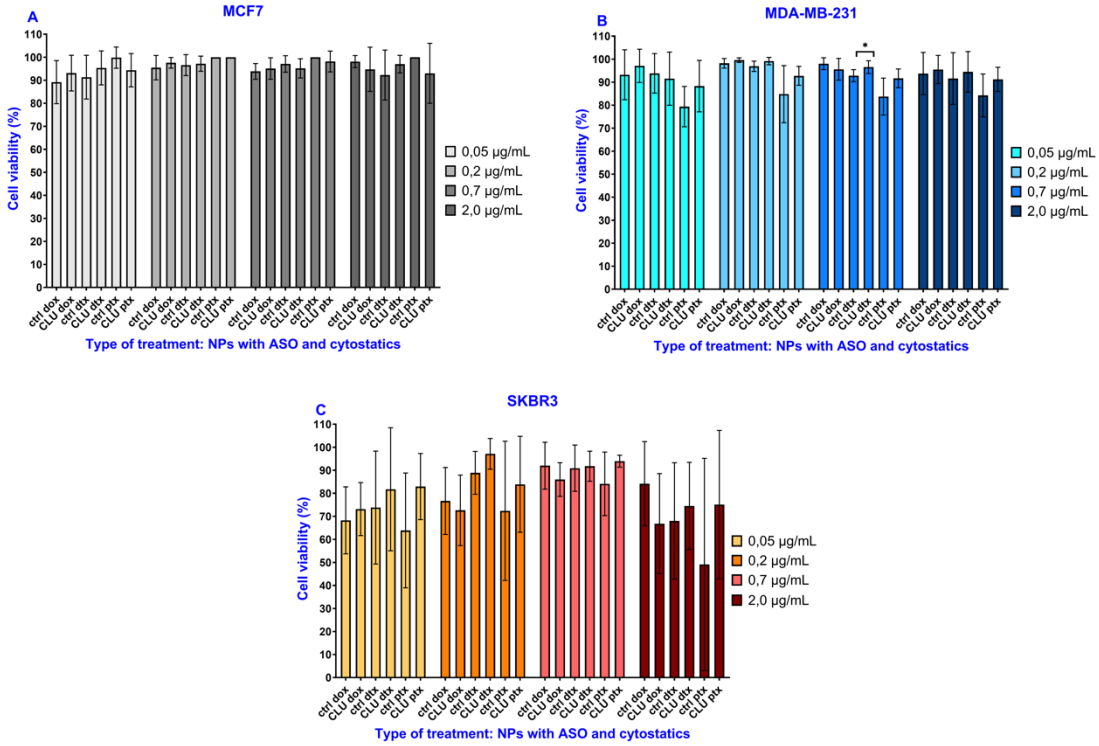

Figure 11 - Graphical representation of cell viability of MCF7, MDA-MB-231 and SKBR3, highlighting the ASO role. Cell viability of: **A)** MCF7; **B)** MDA-MB-231; **C)** SKBR3. ctrl – NPs loaded with OGX-011**R**_2; CLU – NPs loaded with OGX-011**F**_2,

Based on the results from Fig. 7, performed to study cell viability of MCF7, MDA-MB-231 and SKBR3, after treatment with NPs loaded with different concentrations of ASO (OGX-011**F**_2 and OGX-011**R**_2), and followed by treatment with the IC50 concentration of DOX, DTX and PTX for each cell line, a representation of cell viability under a different perspective can be observed. In this assay, one of the controls used referred to cells treated only with one of the cytostatic agents (cells + drug). To plot this graph, the value of the control “cells + drug” was used as the basis for calculating cell viability values of each cell line. This way, the results of cell viability are compared, emphasizing the role of the ASO in different concentrations, since the basis is equal in terms of survival under a specific drug treatment. For each cytostatic agent, in every concentration used, in all cell lines, the p-value between the experimental conditions control *vs* CLU was calculated revealing, in general, no statistically significant reduction of cell viability enabled by clusterin-targeted NPs. These graphs show that cell line SKBR3 is more

sensitive to the combination of treatments, presenting lower cell viability results than the other cell lines, especially at the highest concentration of ASO.

4. Conclusions

The aim of this study was to investigate the physical and biochemical characteristics of PLGA NPs loaded with two different oligonucleotides ASO – OGX-011**R**_2 (control) and OGX-011**F**_2 (CLU) – and to assess their potentiality of sensitizing breast cancer cell lines (MCF7, MDA-MB-231, and SKBR3) to conventional chemotherapeutic agents (doxorubicin, docetaxel, and paclitaxel).

Physical Characterization of PLGA NPs

DLS measurements, showed that PLGA NPs loaded with ASO exhibited a multi-peaked size distribution, indicating that these NPs are polydisperse, showing a tendency for increasing size and aggregation as the ASO's concentration heightens. This tendency was more pronounced in Control NPs than in CLU NPs. In contrast, empty PLGA NPs exhibited high monodispersity, implying a highly uniform size distribution, which was corroborated with TEM images, where empty NPs also appeared with spherical morphology.

Regarding zeta potential measurements, empty PLGA NPs presented a stable and strongly negative charge, while PLGA NPs loaded with ASO presented different surface charges, according to the type of ASO and respective concentrations. While Control NPs tended to show a shift towards a less negative zeta potential as the ASO concentration increased, zeta potential values of CLU NPs tended to be more negative at higher concentrations of the ASO. This suggests a potential reduction in colloidal stability of Control NPs, and conversely, CLU NPs tend to show enhanced stability. However, both types of NPs loaded with ASO, had lower absolute zeta potential values when compared to the empty NPs, indicating that ASO encapsulation has an impact on surface charge, which potentially influences colloidal stability and aggregation predisposition.

Biological Evaluation of PLGA NPs on Breast Cancer Cell Lines

Across the three breast cancer cell lines, MCF7, MDA-MB-231, and SKBR3, biocompatibility of empty PLGA NPs was confirmed, showing no cytotoxicity, revealing that this polymer carrier is potentially safe to use in biological tissues. This result reinforces PLGA's potential as a gene delivery vector for therapeutic applications.

Studies of dose-response with chemotherapeutic agents enhanced different sensitivities among the cell lines, with MCF7 and SKBR3 showing greater sensitivity to doxorubicin and paclitaxel, while MDA-MB-231 exhibited a more resistant phenotype, which is consistent with its subtype of cancer cell (TNBC). In addition, these findings are aligned with the existing literature on chemotherapeutic response across breast cancer subtypes and its variability.

Influence of ASO-Loaded NPs on Chemotherapeutic Sensitization

When breast cancer cells were pre-treated with NPs loaded with ASO and then exposed to the chemotherapeutic agents in study, results showed, a general trend of reduced cell viability with increasing ASO concentration, more pronounced in MDA-MB-231 and SKBR3. However, statistical analysis indicated no significant increasing of sensitivity to chemotherapeutic agents, in any of the cell lines, in the presence of NPs loaded with CLU ASO, when comparing to results of cells treated with Control ASO. Remarkably, SKBR3 cells demonstrated heightened sensitivity to the combined treatment, suggesting that HER2-positive cells may be more responsive to this therapeutic approach, particularly at higher ASO concentrations.

Regardless of these observations, the statistical insignificance in most comparisons suggests that, at the tested ASO concentrations, clusterin-targeted PLGA NPs do not constantly improve chemotherapeutic efficacy, by the cytostatic agents in study. Therefore, further optimization of NPs synthesis process, respective physicochemical characterization and of ASO encapsulation, will be required to reinforce this sensitization effect.

Implications and Future Directions

This study provides valuable insights into the potential of PLGA NPs for ASO delivery, particularly in encapsulating ASO with minor structural differences, though further optimization is needed to accurately assess encapsulation efficiency, which we did not assess. In fact, some more limitations should be acknowledged. Since we did not measure CLU mRNA or protein levels post-treatment, assess NP internalisation, or compare encapsulated with naked ASO, some aspects of their mechanism and efficacy

remain uncertain. Future studies addressing these factors could offer clearer insights into CLU silencing effects and the potential advantages of ASO encapsulation, ultimately supporting the development of more targeted cancer therapies.

The distinctive zeta potential and aggregation patterns observed between the control and CLU NPs, highlight the impact of nucleotide mismatches on NP characteristics, drawing attention to the need of further investigation to optimize stability and drug delivery efficacy.

Even though clusterin-targeted NPs did not enhance chemotherapeutic sensitivity of cell lines in study with statiscal relevance, future work could contemplate alternative encapsulation methods or experimenting higher ASO concentrations. Additionally, exploring other ASO sequences with more substantial differences could reveal whether more pronounced structural variations enhance therapeutic outcomes.

Nevertheless, PLGA NPs remain a promising tool for ASO delivery in breast cancer treatment, although their formulation requires further refinement in order to achieve substantial therapeutic benefits in strategies combining the delivery of ASO with conventional chemotherapeutic treatments.

References

1. Bayda, S., et al., *The History of Nanoscience and Nanotechnology: From Chemical-Physical Applications to Nanomedicine.* Molecules, 2020. **25**(1).
2. Office, N.N.C. *National Nanotechnology Initiative*. 2024 2024 [cited 2024 15/09/2024]; Available from: www.nano.gov.
3. Whitesides, G.M., *Nanoscience, nanotechnology, and chemistry.* Small, 2005. **1**(2): p. 172-179.
4. Binnig, G. and H. Rohrer, *Scanning Tunneling Microscopy - from Birth to Adolescence.* Reviews of Modern Physics, 1987. **59**(3): p. 615-625.
5. Selvan, S.T., et al., *Functional and Multifunctional Nanoparticles for Bioimaging and Biosensing.* Langmuir, 2010. **26**(14): p. 11631-11641.
6. Moghimi, S.M., A.C. Hunter, and J.C. Murray, *Nanomedicine: current status and future prospects.* Faseb Journal, 2005. **19**(3): p. 311-330.
7. Bhatia, S.N., et al., *Cancer nanomedicine.* Nature Reviews Cancer, 2022. **22**(10): p. 550-556.
8. Soares, S., et al., *Nanomedicine: Principles, Properties, and Regulatory Issues.* Frontiers in Chemistry, 2018. **6**.
9. Soares, S., et al., *Nanomedicine: Principles, Properties, and Regulatory Issues.* Front Chem, 2018. **6**: p. 360.
10. Wagner, V., et al., *The emerging nanomedicine landscape.* Nature Biotechnology, 2006. **24**(10): p. 1211-1217.
11. Zhang, C.Y., et al., *Progress, challenges, and future of nanomedicine.* Nano Today, 2020. **35**.
12. Zingg, R. and M. Fischer, *The consolidation of nanomedicine.* Wiley Interdisciplinary Reviews-Nanomedicine and Nanobiotechnology, 2019. **11**(6).
13. Barenholz, Y., *Doxil® - The first FDA-approved nano-drug: Lessons learned.* Journal of Controlled Release, 2012. **160**(2): p. 117-134.
14. Freitas, R.A., *What is nanomedicine?* Nanomedicine: Nanotechnology, Biology and Medicine, 2005. **1**(1): p. 2-9.
15. Guidolin, K. and G. Zheng, *Nanomedicines Lost in Translation.* Acs Nano, 2019. **13**(12): p. 13620-13626.
16. Fan, D.H., et al., *Nanomedicine in cancer therapy.* Signal Transduction and Targeted Therapy, 2023. **8**(1).
17. Gmeiner, W.H. and S. Ghosh, *Nanotechnology for cancer treatment.* Nanotechnology Reviews, 2014. **3**(2): p. 111-122.
18. Fonseca, D.R., et al., *One-Pot Microfluidics to Engineer Chitosan Nanoparticles Conjugated with Antimicrobial Peptides Using "Photoclick" Chemistry: Validation Using the Gastric Bacterium.* Acs Applied Materials & Interfaces, 2024. **16**(12): p. 14533-14547.
19. Geng, W.C., et al., *Supramolecular interaction in the action of drug delivery systems.* Chemical Science, 2024. **15**(21): p. 7811-7823.
20. Makadia, H.K. and S.J. Siegel, *Poly Lactic-co-Glycolic Acid (PLGA) as Biodegradable Controlled Drug Delivery Carrier.* Polymers, 2011. **3**(3): p. 1377-1397.
21. Danhier, F., et al., *PLGA-based nanoparticles: An overview of biomedical applications.* Journal of Controlled Release, 2012. **161**(2): p. 505-522.
22. Gaspar, L.M.D.C., et al., *Development and characterization of PLGA nanoparticles containing antibiotics.* Journal of Nanoparticle Research, 2018. **20**(11).

23. Hapuarachchige, S. and D. Artemov, *Theranostic Pretargeting Drug Delivery and Imaging Platforms in Cancer Precision Medicine.* Frontiers in Oncology, 2020. **10**.
24. Nimmagadda, S. and M.F. Penet, *Ovarian Cancer Targeted Theranostics.* Front Oncol, 2019. **9**: p. 1537.
25. Soliman, G.M., et al., *Dendrimers and miktoarm polymers based multivalent nanocarriers for efficient and targeted drug delivery.* Chemical Communications, 2011. **47**(34): p. 9572-9587.
26. Briolay, T., et al., *Delivery of cancer therapies by synthetic and bio-inspired nanovectors.* Molecular Cancer, 2021. **20**(1).
27. dos Santos, T., et al., *Effects of Transport Inhibitors on the Cellular Uptake of Carboxylated Polystyrene Nanoparticles in Different Cell Lines.* Plos One, 2011. **6**(9).
28. Salvati, A., et al., *Experimental and theoretical comparison of intracellular import of polymeric nanoparticles and small molecules: toward models of uptake kinetics.* Nanomedicine, 2011. **7**(6): p. 818-26.
29. Wu, J., *The Enhanced Permeability and Retention (EPR) Effect: The Significance of the Concept and Methods to Enhance Its Application.* Journal of Personalized Medicine, 2021. **11**(8).
30. García-Aranda, M., et al., *Clusterin inhibition mediates sensitivity to chemotherapy and radiotherapy in human cancer.* Anti-Cancer Drugs, 2017. **28**(7): p. 702-716.
31. Martín-García, D., M. García-Aranda, and M. Redondo, *Therapeutic Potential of Clusterin Inhibition in Human Cancer.* Cells, 2024. **13**(8).
32. Redondo, M., et al., *Downregulation of clusterin mediates sensitivity to protein kinase inhibitors in breast cancer cells.* Anti-Cancer Drugs, 2015. **26**(1): p. 85-89.
33. Tellez, T., M. Garcia-Aranda, and M. Redondo, *The Role of Clusterin in Carcinogenesis and its Potential Utility as Therapeutic Target.* Current Medicinal Chemistry, 2016. **23**(38): p. 4297-4308.
34. García-Aranda, M., A. Serrano, and M. Redondo, *Regulation of Clusterin Gene Expression.* Current Protein & Peptide Science, 2018. **19**(6): p. 612-622.
35. Hernandez-Giottonini, K.Y., et al., *PLGA nanoparticle preparations by emulsification and nanoprecipitation techniques: effects of formulation parameters.* RSC Adv, 2020. **10**(8): p. 4218-4231.
36. Martins, C., et al., *Stimuli-Responsive Multifunctional Nanomedicine for Enhanced Glioblastoma Chemotherapy Augments Multistage Blood-to-Brain Trafficking and Tumor Targeting.* Small, 2023. **19**(22).
37. Chi, K.N., et al., *A Phase I Pharmacokinetic and Pharmacodynamic Study of OGX-011, a 2'-Methoxyethyl Antisense Oligonucleotide to Clusterin, in Patients With Localized Prostate Cancer.* JNCI: Journal of the National Cancer Institute, 2005. **97**(17): p. 1287-1296.
38. Uhlén, M., et al., *The human secretome.* Sci Signal, 2019. **12**(609).
39. Royal Institute of Technology in Stockholm, U.U., Uppsala Akademiska University Hospital, Science for Life Laboratory in Uppsala and Stockholm. *The Human Protein Atlas*. 19/06/2023 11/09/2024]; Available from: https://www.proteinatlas.org.
40. Bilardo, R., et al., *Influence of surface chemistry and morphology of nanoparticles on protein corona formation.* Wiley Interdisciplinary Reviews-Nanomedicine and Nanobiotechnology, 2022. **14**(4).
41. Serrano-Lotina, A., et al., *Zeta potential as a tool for functional materials development?* Catalysis Today, 2023. **423**.

42. Honary, S. and F. Zahir, *Effect of Zeta Potential on the Properties of Nano-Drug Delivery Systems - A Review (Part 2).* Tropical Journal of Pharmaceutical Research, 2013. **12**(2): p. 265-273.
43. Zhang, Y., et al., *Zeta potential: a surface electrical characteristic to probe the interaction of nanoparticles with normal and cancer human breast epithelial cells.* Biomedical Microdevices, 2008. **10**(2): p. 321-328.
44. Bhattacharjee, S., *DLS and zeta potential – What they are and what they are not?* Journal of Controlled Release, 2016. **235**: p. 337-351.
45. Xie, J., S. Lee, and X.Y. Chen, *Nanoparticle-based theranostic agents.* Advanced Drug Delivery Reviews, 2010. **62**(11): p. 1064-1079.
46. Minea, A.A., *A Review on Electrical Conductivity of Nanoparticle-Enhanced Fluids.* Nanomaterials, 2019. **9**(11).
47. Chereches, E.I. and A.A. Minea, *Electrical Conductivity of New Nanoparticle Enhanced Fluids: An Experimental Study.* Nanomaterials, 2019. **9**(9).
48. Alberts, B., Johnson, A., Lewis, J., et al., *"Molecular Biology of the Cell" (6th Edition)*. 2014: Garland Science.
49. Begines, B., et al., *Polymeric Nanoparticles for Drug Delivery: Recent Developments and Future Prospects.* Nanomaterials, 2020. **10**(7).
50. Terada, C., et al., *Chemistry of Therapeutic Oligonucleotides That Drives Interactions with Biomolecules.* Pharmaceutics, 2022. **14**(12).
51. Alsaab, H.O., et al., *PLGA-Based Nanomedicine: History of Advancement and Development in Clinical Applications of Multiple Diseases.* Pharmaceutics, 2022. **14**(12).
52. Howard, G.R., et al., *Quantification of long-term doxorubicin response dynamics in breast cancer cell lines to direct treatment schedules.* Plos Computational Biology, 2022. **18**(3).
53. Xu, F.F., et al., *Differential drug resistance acquisition to doxorubicin and paclitaxel in breast cancer cells.* Cancer Cell International, 2014. **14**.
54. Christowitz, C., et al., *Mechanisms of doxorubicin-induced drug resistance and drug resistant tumour growth in a murine breast tumour model.* Bmc Cancer, 2019. **19**(1).